Journal of Catalysis **192,** 29–47 (2000)
doi:10.1006/jcat.2000.2846, available online at http://www.idealibrary.com on IDEAL®

Adsorption and Decomposition of NO on Lanthanum Oxide

S.-J. Huang, A. B. Walters, and M. A. Vannice[1]

Department of Chemical Engineering, The Pennsylvania State University, University Park, Pennsylvania 16802

Received July 23, 1999; revised February 9, 2000; accepted February 11, 2000

The adsorption behavior of NO on La_2O_3, an effective catalyst for selective NO reduction with CH_4 at temperatures above 800 K, depends upon the pretreatment as indicated by temperature-programmed desorption (TPD) and diffuse reflectance FTIR spectroscopy (DRIFTS). The use of isotopic $^{18}O_2$ exchange and adsorption showed that oxygen adsorbed dissociatively by filling oxygen vacancies and that both oxygen vacancies and lattice oxygen were mobile at high temperature. Oxygen pair vacancies were assumed to be created by desorption of molecular oxygen and, upon cooling, a certain distribution of pair and single vacancies exists at the surface as the pair vacancies can rearrange due to oxygen ion migration. After La_2O_3 was pretreated at 973 K in He, exposure to NO at 300 K caused a brief reaction forming N_2O, then gave three NO TPD peaks at 400, 700, and 800 K. The only O_2 desorption occurred during the 800 K NO peak and gave an NO/O_2 ratio near unity. Oxygen chemisorption prior to NO admission eliminated the formation of N_2O during NO adsorption at 300 K, blocked the sites giving NO desorption at 700 K, but enhanced the NO and O_2 peaks at 800 K. TPD after $^{15}N^{16}O$ adsorption on an La_2O_3 surface containing exchanged ^{18}O lattice anions, but no chemisorbed O atoms, showed that both $^{15}N^{16}O$ and $^{15}N^{18}O$ desorbed at 400 K, but only $^{15}N^{16}O$ was present in the 700 and 800 K desorption peaks, and $^{16}O_2$ again desorbed at 800 K. When both lattice exchange and chemisorption of $^{18}O_2$ on the La_2O_3 surface were allowed before $^{15}N^{16}O$ adsorption, $^{15}N^{18}O$ was desorbed at 400 and 800 K while $^{16}O_2$, $^{16}O^{18}O$, and $^{18}O_2$ were also desorbed at 800 K; thus the NO peak at 400 K involves exchange with surface lattice oxygen atoms, while the 800 K peak involves exchange with chemisorbed oxygen atoms. DRIFTS indicated the presence of anionic nitrosyl (NO^-), hyponitrite $(N_2O_2)^{2-}$, chelated nitrite (NO_2^-), nitrito (ONO^-), and bridging and monodenate nitrate (NO_3^-) species. Consequently, the three NO TPD peaks were assigned as follows: 400 K, decomposition of nitrito, nitro, and bidentate nitrate species; 700 K, desorption from NO^- and $(N_2O_2)^{2-}$ species; and 800 K, decomposition of monodenate nitrate species into NO and O_2. A model of the La_2O_3 surface based on the (001) and (011) crystal planes is proposed to account for these different sites. Two types of oxygen pair vacancy sites with a different O–O separation appear to exist, with one forming $(N_2O_2)^{2-}$ species, and four additional sites—(1) an oxygen single vacancy, (2) a single vacancy and a lattice oxygen atom, (3) a coordinative unsaturated lattice oxygen atom, and (4) adjacent lattice oxygen atoms—are proposed to explain the formation of NO^-, nitrito (M–ONO^-), chelated nitrites, and bridging nitrate species, respectively. Among these species, $(N_2O_2)^{2-}$ was detected by DRIFTS under reaction conditions at 800 K and is most likely to be an active intermediate during NO decomposition. Monodentate nitrate species are also observed at 800 K, but are very stable and still present after purging at 800 K.

INTRODUCTION

The emission of NO_x from both mobile and stationary sources is a serious environmental problem, thus NO_x decomposition and reduction has drawn much attention in catalysis, especially for treating exhaust gases produced under lean-burn conditions. La_2O_3, an effective catalyst for oxidative coupling of methane, has been shown to be active and selective for NO reduction by CH_4 in excess O_2 (1, 2), and when CO or H_2 is used as a reductant, La_2O_3 exhibits higher specific activity, but it is not selective in excess O_2 (3). Although the kinetic behavior of NO reduction over La_2O_3 has been investigated in some depth (4), limited attention has been given to the surface chemistry associated with the adsorption and reaction of NO on La_2O_3 (3–7). Studies using infrared spectroscopy have shown that a variety of adsorbed NO species can exist on La_2O_3 (5), and NO can interact with both surface oxygen vacancies and lattice oxygen to form a multiplicity of adsorbed species. TPD using a lanthana film prepared by spray pyrolysis onto an aluminum single crystal showed that this film, which was reduced by CO, was capable of adsorbing both CO and NO and catalyzing the formation of N_2O and N_2 from NO (6). Nevertheless, the preparation and pretreatment of La_2O_3 can significantly affect its surface properties and, consequently, its adsorption and catalytic behavior (8–10). The use of NO and O_2 as probe molecules to obtain information about adsorption sites on La_2O_3 surfaces can provide a better understanding of the surface chemistry involved during NO decomposition and reduction on La_2O_3. In the present study, the interaction of NO and O_2 with La_2O_3 surfaces after different pretreatments was studied by temperature-programmed desorption (TPD) and diffuse reflectance FTIR spectroscopy (DRIFTS). Isotopically labeled ^{15}NO and $^{18}O_2$ were also used to clarify the interaction of NO with chemisorbed surface oxygen atoms as well as

[1] To whom correspondence should be addressed.

0021-9517/00 $35.00

surface lattice oxygen atoms. Surface species produced during NO adsorption on an La_2O_3 sample prepared after pretreatments used in kinetic studies were characterized by TPD and DRIFTS to allow direct comparison. The NO TPD peaks were used to establish temperatures to which the sample could be heated in the DRIFTS cell to remove certain portions of the adsorbed species, thus facilitating their identification. In addition, a model of the La_2O_3 surface is proposed which accounts for the different sites required to form the observed surface NO_x species and is relevant to the surface chemistry associated with NO decomposition on La_2O_3.

EXPERIMENTAL

The La_2O_3 sample was prepared by calcining a commercial La_2O_3 powder (99.99%, Rhone-Poulenc Inc.) at 1023 K under flowing O_2 at 50 cm^3(STP)/min for 10 h. The sample was stored in a desiccator after calcination. The BET surface area of the La_2O_3 sample described here was 2.4 m^2/g. Another sample with a lower surface area of 0.72 m^2/g was also studied (11), but both the TPD spectra and the specific activity for N_2 formation were so similar that only the former sample is emphasized.

The TPD experiments were performed at 1 atm using a small fixed bed of sample (ca. 240 mg) placed in a 30-cm-long, 4-mm-i.d. quartz tube. The temperature ramp was controlled by an Omega CN 2011 temperature controller. The evolved gases were analyzed continuously with a UTI 100C quadrupole mass spectrometer using an ionization voltage of 70 eV. The gases used were UHP grade He (99.999%), 4.01% NO/He, 3.83% H_2/He, and 10% O_2/He (all from MG Industries), CO_2 (99.995%, BOC Group, Inc.), and 0.509% N_2O/Ar (Matheson). The desired gas concentration was achieved by further mixing with pure He. NO was passed through both an Ascarite trap and a Drierite trap to strip CO_2 and moisture. He and O_2 were passed through a molecular sieve moisture trap. Isotopically labeled ^{15}NO was from either Isotec Inc. (99%) or Cambridge Isotope Laboratories (98%), and $^{18}O_2$ was obtained from Isotec Inc. (99.2%).

The typical TPD procedure was as follows, unless stated otherwise. Prior to the NO TPD experiments, the catalyst was treated in one of the following three ways: (1) by flowing He at 30 cm^3/min at 973 K for 1 h and cooling to 300 K in He (denoted as He treatment); (2) by flowing 10% O_2/He at 30 cm^3/min at 973 K for 1 h, cooling to 300 K in 10% O_2/He, and purging in He at 300 K (O_2 treatment); or (3) by flowing 3.83% H_2/He at 973 K for 1 h, then cooling in 3.83% H_2 and purging in He at 300 K (H_2 treatment). This latter pretreatment was conducted to determine the effect of cooling under H_2 on the state of the La_2O_3 surface. The adsorbate gas was fed into the reactor at a flow rate of 20 cm^3/min at 300 K for 30 min, followed by purging with He until the background signals monitored by the mass spectrometer reached a steady state. During the TPD runs, a carrier gas flow of 30 cm^3 He/min was passed through the reactor at a linear heating rate of 50 K/min from 300 to 973 K. A small portion of the effluent gas was introduced into the mass spectrometer through a needle valve allowing control of the pressure inside the mass spectrometer chamber at 10^{-7} Torr. Quantitative analyses for NO, O_2, and N_2 were obtained by the area integration under each peak profile which was corrected by its respective sensitivity factor. Because it was found that the signal sensitivities of NO and O_2 were dependent on their concentrations, NO and O_2 signal sensitivities at various concentrations with respect to He were calibrated to minimize the uncertainty in calculating the amount of desorbing species. A concomitant N_2 signal was found to occur with the NO signal because of NO decomposition on the hot filament in the mass spectrometer; however, due to the N_2 impurity in the NO source, an accurate measurement of N_2 formation from this decomposition was not possible, and therefore the extent of NO decomposition in the mass spectrometer was determined by a GC–MS experiment in order to separate the N_2 impurity from the NO gas source. Cracking patterns for the various gases were also experimentally determined, and the detailed calibration procedures are provided elsewhere (11).

TPD of $^{16}O_2$ was performed after the O_2 treatment previously described, but TPD after $^{18}O_2$ adsorption was carried out using the following procedure. La_2O_3 was pretreated in He at 973 K for 1 h, evacuated for 20 min, then 1 atm of $^{18}O_2$ was admitted into the evacuated reactor to allow adsorption in a closed system as it was cooled from 973 to 300 K. The $^{18}O_2$ was used to generate two states of the La_2O_3 surface: (1) one with a limited amount of ^{18}O surface lattice oxygen due to exchange with $^{18}O_2$, designated $La_2^{16,18}O_3$, and (2) one with chemisorbed ^{18}O as well as lattice ^{18}O ions, designated $La_2^{16,18}O_3(^{16,18}O)$, where the oxygen inside the parentheses indicates chemisorbed oxygen atoms. The former was produced by exposing an La_2O_3 sample at 500 K to a series of 10 pulses of $^{18}O_2$ at 500 K in flowing He. The latter was obtained by admitting 1 atm of $^{18}O_2$ into a closed and pre-evacuated reactor containing La_2O_3 at 973 K and allowing the adsorption and exchange processes to proceed as the sample was cooled to 300 K. Isotopic ^{15}NO was used to differentiate species with the same m/e ratios, such as $^{14}N^{18}O$ and $^{16}O_2$ ($m/e = 32$), $^{14}N_2O$ and CO ($m/e = 28$), and $^{14}N_2$ and CO_2 ($m/e = 44$). The isotopic gas was introduced into the reactor by pulses carried by a He flow of 20 cm^3/min and switched by a six-port valve with a 250-μl sample loop. The TPD experiments were conducted using the same procedure as described earlier.

A series of pulsed $^{18}O_2$ exchange experiments was carried out with La_2O_3 after each of the following three pretreatments: (a) heat in flowing He at 973 K for 1 h and cool to 500 K in He; (b) heat in a flowing mixture of 9.9% O_2 in He

at 973 K for 1 h, cool to 500 K in O_2, then purge with He for 10 min; and (c) heat in flowing He at 973 K for 1 h, cool to 500 K, then expose to NO at 500 K. The $^{18}O_2$ exchange reaction was carried out by injection of 250-μl pulses of $^{18}O_2$ into 20 cm^3 He/min passing through the catalyst at 500 K, and the contents of the effluent gas were analyzed by mass spectrometry. After each of these three pulsed $^{18}O_2$ exchange experiments, the sample was cooled to 300 K in He and a TPD experiment using He as the carrier gas was performed. After the TPD run, the sample treated in either He (case a) or O_2 (case b) was cooled again to 300 K in He and a temperature-programmed isotopic O_2 exchange (TPIE) was carried out by using a carrier gas of 5% $^{16}O_2$ in He instead of pure He to see if exchange with ^{18}O lattice ions would occur on the La_2O_3 surface.

Diffuse reflectance Fourier transform infrared spectroscopy (DRIFTS) was conducted with a Mattson Research Series 10000 FTIR equipped with an MCT narrowband detector (750–4000 cm^{-1}). A diffuse reflection attachment (Harrick Scientific-DRA) with NaCl windows was connected to a gas handling system to allow measurements under controlled gas environments and temperatures (up to 800 K in flowing Ar). Interferograms were based on 1000 scans at a resolution of 4 cm^{-1}, and data acquisition and processing were performed with commercial Winfirst software (5). The gases used were UHP grade Ar (99.999%), H_2 (99.999%), O_2 (99.999%), 10.0% O_2/90.0% Ar (all from MG Ind.), 4.11% NO in Ar (Matheson), and CO_2 (99.995%, BOC Group, Inc.). Ar was passed through a UOP Model P100 purifier and the 4.11% NO in Ar and 10.0% O_2 in Ar mixtures were passed through Ascarite traps to remove CO_2. The gases were fed under atmospheric pressure in all pretreatments and experiments.

After calcination at 1023 K, the La_2O_3 was stored in a drybox under N_2. Prior to loading in the DRIFTS cell, the La_2O_3 sample was pretreated *ex situ* under flowing He (30 cm^3/min) at 973 K for 1 h, transferred into the IR cell inside the drybox, and closed off before moving to the spectrometer cavity. Inside the DRIFTS cell, temperatures above 800 K could not be achieved, so the TPD pretreatments were approximated by one of the following pretreatments: (1) heat under flowing Ar (50 cm^3/min) to 800 K, hold for 1 h (Ar treatment), then cool; (2) heat under flowing 10% O_2/90% Ar (50 cm^3/min) to 800 K, hold for 1 h, then cool to 300 K in 10% O_2 before purging in Ar for 30 min (O_2 treatment); or (3) heat under flowing 30% H_2/70% Ar (50 cm^3/min) to 800 K and hold for 30 min, purge in Ar for another 30 min at 800 K, then cool (H_2 treatment). To study irreversible NO adsorption, 4.11% NO in Ar was flowed through the La_2O_3 sample at 300 K, then an Ar purge was used. To examine the thermal stability of the various surface species, the sample was heated to either 473, 673, or 800 K under flowing Ar, then cooled from the respective temperature to 300 K at which time the DRIFT spectra were taken. All the spectra were referenced to the catalyst under an Ar purge just prior to exposure to NO at 300 K. DRIFT spectra of adsorbed NO at elevated temperatures were also obtained after flowing 4.11% NO in Ar over an La_2O_3 sample at 473, 673, or 800 K, with the IR spectra being referenced to the background spectrum of the sample at the corresponding temperature prior to exposure to NO because spectra at higher temperatures can exhibit line broadening, peak shifts, and decreases in intensity compared to those at 300 K. All spectra are represented in the absorbance mode, rather than in Kubelka–Munk units, so that losses in band intensity can be seen.

RESULTS

The O_2 TPD spectrum shown in Fig. 1a was obtained after an O_2 treatment, which would be expected to maximize oxygen concentration in bulk La_2O_3 and on the surface. At 630 K, O_2 desorbed giving an amount of 1.0 μmol/m^2. Exposure to O_2 at either 300 or 500 K followed by cooling in He to 300 K gave no O_2 desorption peak from the consecutive O_2 TPD experiments. Adsorption of $^{18}O_2$ was carried out by exposing La_2O_3 to 1 atm of $^{18}O_2$ at 973 K then cooling to 300 K in a closed reactor. The 650 K desorption peak contained not only $^{18}O_2$ but also $^{16}O^{18}O$ and $^{16}O_2$, as shown in Fig. 1b, indicating that O_2 adsorption is dissociative and that the exchange reaction between gas-phase $^{18}O_2$ and lattice ^{16}O occurs. The migration of chemisorbed oxygen

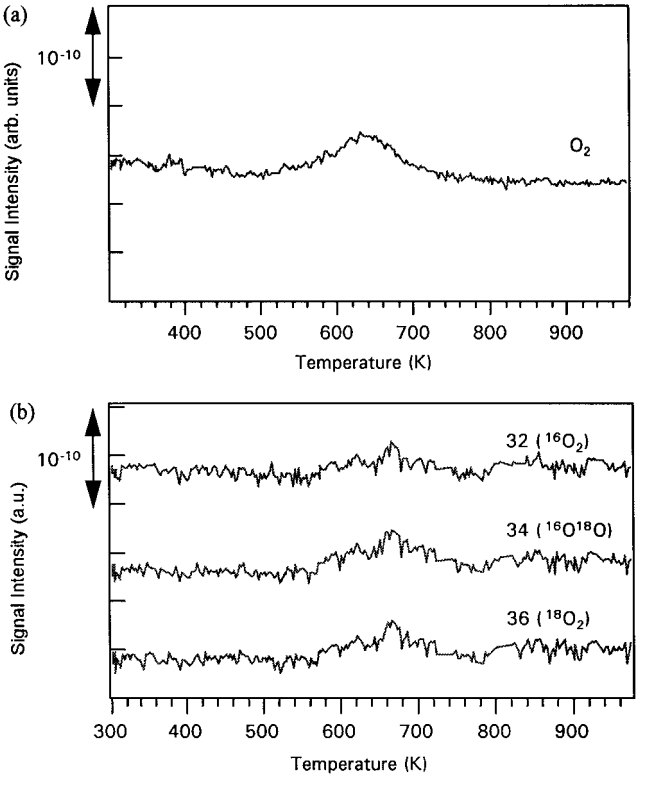

FIG. 1. O_2 TPD from La_2O_3 surface after (a) adsorption of $^{16}O_2$ and (b) adsorption of $^{18}O_2$.

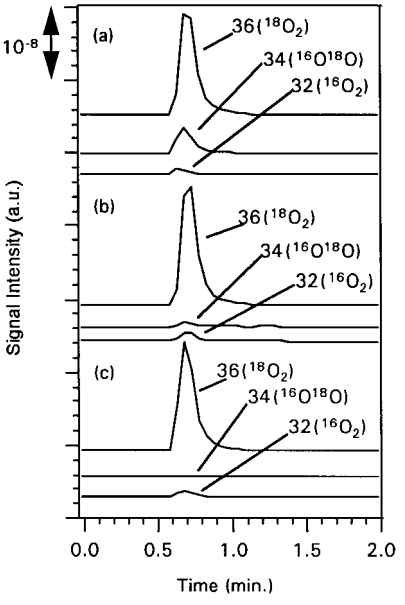

FIG. 2. Pulsed $^{18}O_2$ exchange experiments on La_2O_3 at 500 K (a) after He pretreatment, (b) after O_2 pretreatment, and (c) after He pretreatment with NO preadsorbed at 500 K.

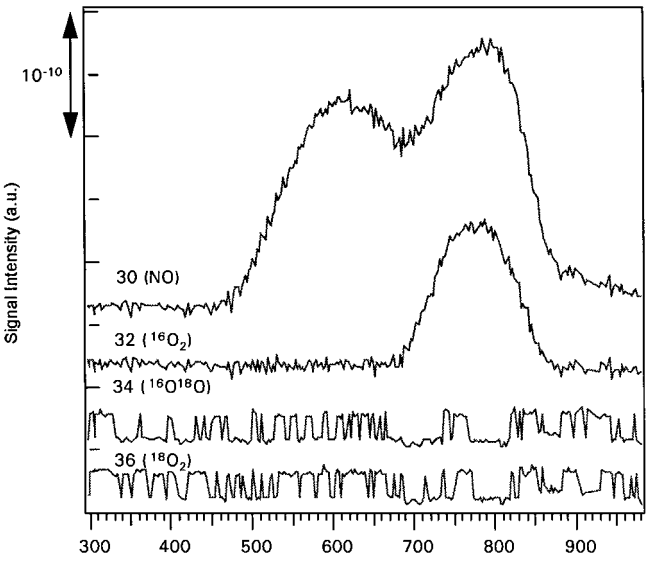

FIG. 3. TPD spectra from La_2O_3 after NO was first adsorbed at 500 K and then the surface was exposed to $^{18}O_2$ at 500 K. No exchange reaction occurred between the adsorbed NO species and $^{18}O_2$.

atoms and lattice oxygen can also take place at high temperatures during the adsorption/desorption processes.

A series of $^{18}O_2$ exchange experiments was carried out to learn about the influence of preadsorbed atoms on an La_2O_3 surface on the oxygen exchange ability as well as the nature of the adsorption/exchange sites. The pulsed $^{18}O_2$ exchange reaction was performed at 500 K because O_2 starts to desorb at this temperature. As can be seen in Fig. 2, the amount of the $^{18}O^{16}O$ exchange product was greater on the sample treated in He than on the one treated in O_2. The He treatment at 973 K would be expected to result in a relatively high oxygen vacancy concentration in the La_2O_3. No $^{18}O^{16}O$ was observed with the sample containing preadsorbed NO. Subsequent pulses of $^{18}O_2$ to each sample showed similar results, and the $^{18}O^{16}O/^{18}O_2$ signal ratios were about the same. The $^{18}O^{16}O/^{18}O_2$ ratio was from 0.31 to 0.36 for the sample treated in He, 0.02 to 0.04 for the sample treated in O_2, and essentially zero for the sample with preadsorbed NO. In these three cases, the formation and desorption of $^{16}O_2$ was negligible because the signal intensity for mass 32 in the effluent was similar to that determined directly from the isotope source after bypassing the La_2O_3 bed. After each of these pulsed O_2 exchange experiments, the reactor was cooled to 300 K under He and a TPD experiment was performed. No distinguishable desorption peak for either $^{18}O_2$, $^{18}O^{16}O$, or $^{16}O_2$ was observed during TPD runs with the samples treated in He or O_2 (not shown), thus verifying previous results that no net irreversible oxygen adsorption occurs at 500 K or below. For the sample with preadsorbed NO, NO desorption peaks were observed at 600 and 800 K, and an $^{16}O_2$ peak was also observed concomitantly with the NO peak at 800 K, as shown in Fig. 3. The temperature-programmed isotopic O_2 exchange (TPIE) runs after the TPD experiments show that the exchange reaction begins near 600 K on the He-treated La_2O_3 with an increase in the $^{16}O^{18}O$ signal intensity (Fig. 4a), whereas for the O_2-treated La_2O_3 (Fig. 4b), only a very small amount of $^{16}O^{18}O$ was evolved during the TPIE experiment.

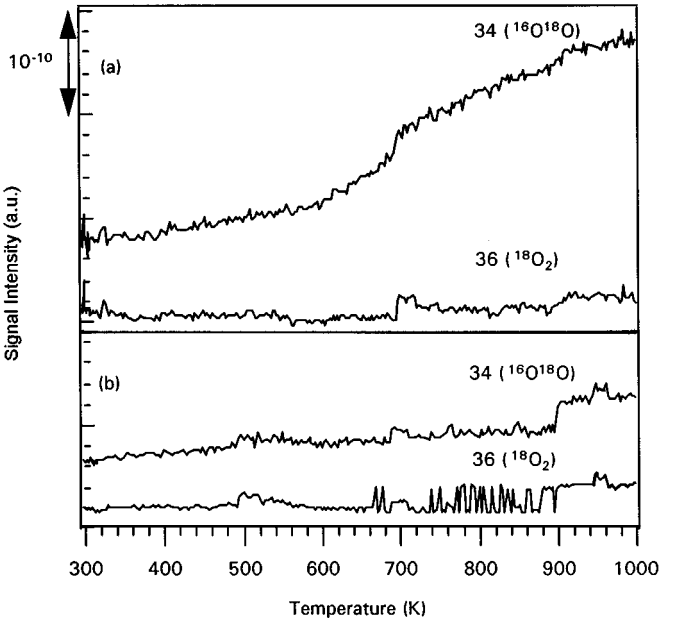

FIG. 4. Temperature-programmed isotopic exchange (TPIE) for La_2O_3 exchanged with ^{18}O at 500 K: (a) He-pretreated La_2O_3 and (b) O_2-pretreated La_2O_3. No $^{16}O_2$ was observed in either case. Carrier gas: 5% $^{16}O_2$–90% He.

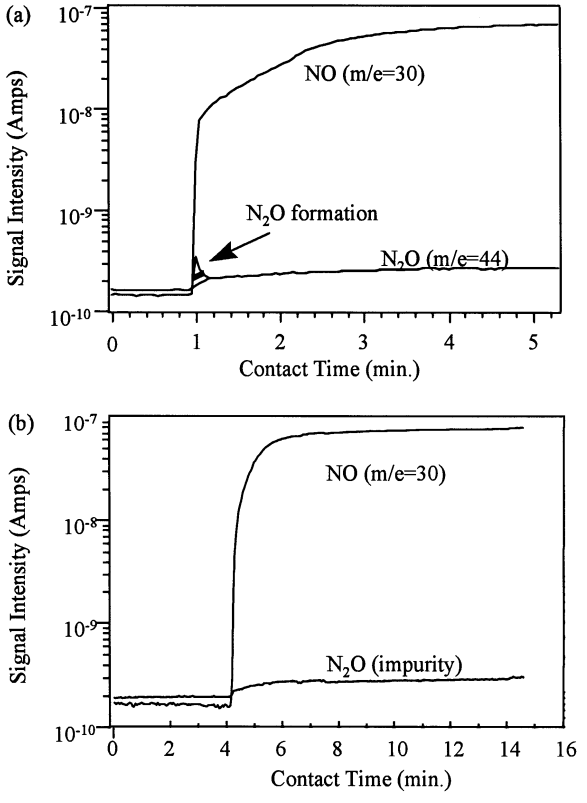

FIG. 5. N_2O formation upon initial contact of NO with La_2O_3: (a) He-treated and (b) O_2-treated.

Exposure of La_2O_3 to NO at 300 K after the He pretreatment produced a small amount of excess N_2O (0.05 μmol/m^2), as shown in Fig. 5, before dropping to its steady-state impurity level in the NO. No N_2 was formed in the same manner as N_2O, and the rise of the N_2 signal (not shown) was due to the N_2 impurity as well as NO decomposition on the filament. The NO TPD spectra for the He-, O_2-, and H_2-pretreated surfaces are shown in Fig. 6. For NO TPD from He-treated La_2O_3, three distinctive NO desorption peaks at 400, 700, and 800 K were observed, and O_2 desorbed at 800 K with the NO, instead of at 620 K as observed in the O_2 TPD. The amounts of O_2 and NO desorbed at 800 K repeatedly gave a molar ratio near unity (see Table 1). The O_2 pretreatment prior to NO adsorption gave only two NO desorption peaks at 400 and 800 K, and the O_2 again desorbed at 800 K coincidently with the NO peak; however, this O_2 pretreatment significantly enhanced the NO and O_2 desorption peaks at 800 K. After the H_2 pretreatment, only a small amount of NO, if any, was detected at 700 K. N_2, NO_2, and N_2O were not formed in detectable amounts during the NO TPD experiments after any of the three different pretreatments. The amounts of NO and O_2 desorbed from the La_2O_3 surface after either an He or an O_2 pretreatment are listed in Table 1. TPD of NO from a sample pretreated in O_2 or H_2 at 973 K, but purged in He at

TABLE 1

NO and O_2 Desorption from La_2O_3 during TPD after Exposure to (a) 4% NO or (b) NO + O_2 at 300 K

(a) After He pretreatment

Temperature (K)	NO desorbed (μmol/m^2)	NO coverage[a] (%)	O_2 desorbed (μmol/m^2)
400	2.6	13	—
700	0.5	2.5	—
800	0.17	0.8	0.17

After O_2 pretreatment

Temperature (K)	NO desorbed (μmol/m^2)	NO coverage[a] (%)	O_2 desorbed (μmol/m^2)
400	3.4	17	—
700	—	—	—
800	3.3	16	3.1

(b) After He pretreatment

Temperature (K)	NO desorbed (μmol/m^2)	O_2 desorbed (μmol/m^2)	N_2 desorbed (μmol/m^2)	Adsorbed NO_x coverage[a] (%)
400	0.15	—	—	0.8
800	8.5	8.7	0.8	44

After O_2 pretreatment

Temperature (K)	NO desorbed (μmol/m^2)	O_2 desorbed (μmol/m^2)	N_2 desorbed (μmol/m^2)	Adsorbed NO_x coverage[a] (%)
400	0.1	—	—	0.5
800	9.7	10.6	1.0	50

[a]Assuming surface monolayer = 1.2×10^{19} molecules/m^2.

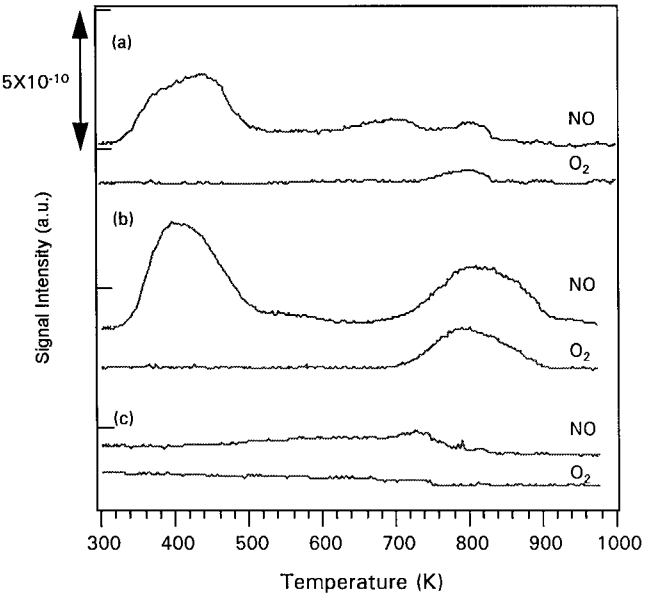

FIG. 6. TPD spectra of NO from (a) He-treated, (b) O_2-treated, and (c) H_2-treated La_2O_3.

700 K before further cooling, gave the same result as that after a He pretreatment (11).

To investigate interactions between adsorbed NO and chemisorbed oxygen or lattice oxygen atoms on the La_2O_3 surface, ^{15}NO and $^{18}O_2$ were used for adsorption. As mentioned before, only after exposure to O_2 continuously during cooling from 973 to 300 K was a distinct O_2 desorption peak obtained. Introduction of O_2 pulses at 500 K merely contributed to exchange of atoms between gas-phase O_2 and the lattice oxygen at the surface; therefore, introduction of pulses of $^{18}O_2$ at 500 K gave an $La_2^{16,18}O_3$ surface with both ^{16}O and ^{18}O lattice atoms. In contrast, La_2O_3 with chemisorbed ^{18}O atoms was obtained by exposure to $^{18}O_2$ from 973 to 300 K; however, during adsorption the exchange reaction also took place to give a surface with a slight stoichiometric excess of oxygen, designated as $La_2^{16,18}O_3(^{16,18}O)$.

Figure 7 shows results after $^{15}N^{16}O$ adsorption on an $La_2^{16,18}O_3$ surface created by interaction on La_2O_3 with $^{18}O_2$ at 500 K, but with no net oxygen adsorption. The isotopic ^{15}NO was introduced by pulse injection of ^{15}NO into the carrier gas and saturated adsorption was not achieved; therefore, the signal intensities were much weaker than those obtained from normal NO TPD runs. Nevertheless, molecular $^{15}N^{16}O$ was again desorbed at 400, 700, and 800 K; however, $^{15}N^{18}O$ was also contained in the low-temperature (400 K) NO desorption peak, thus implying an exchange reaction between $^{15}N^{16}O$ and surface lattice ^{18}O at this particular adsorption site. No $^{15}N^{18}O$ desorbed at 700 and 800 K. Molecular $^{16}O_2$ also desorbed at 800 K, but neither $^{16}O^{18}O$ nor $^{18}O_2$ was detected.

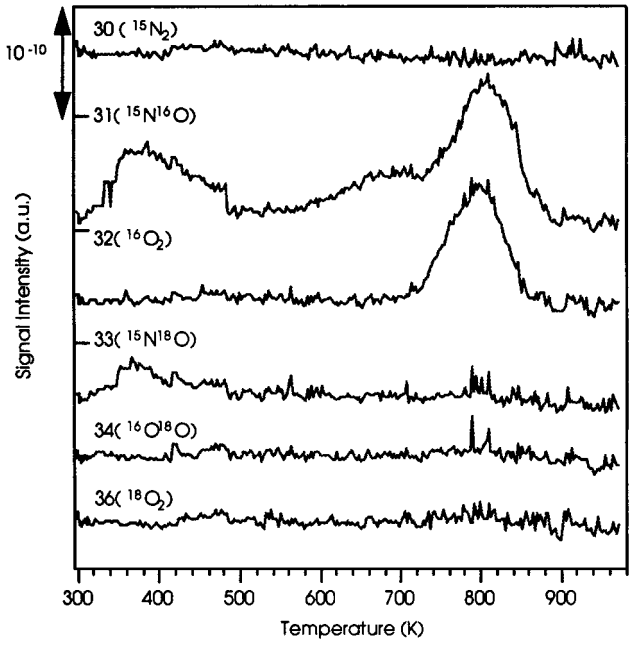

FIG. 7. Desorption of ^{15}NO from an $La_2^{16,18}O_3$ surface. Isotopic $^{18}O_2$ exchange was performed at 500 K prior to ^{15}NO adsorption at 300 K.

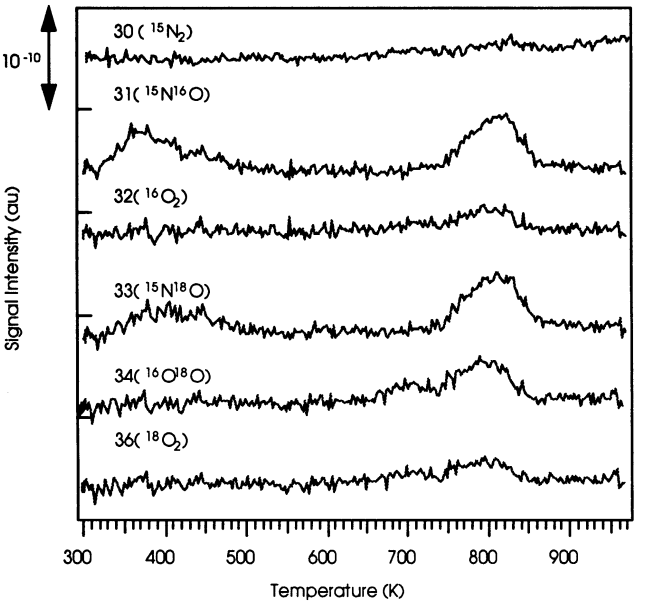

FIG. 8. ^{15}NO desorption from an La_2O_3 surface with chemisorbed ^{18}O $La_2^{16,18}O_3(^{16,18}O)$. $^{18}O_2$ was adsorbed during contact with La_2O_3 while cooling from 973 to 300 K in a closed reactor.

The adsorption of $^{15}N^{16}O$ at 300 K on an $La_2^{16,18}O_3(^{16,18}O)$ surface which contained chemisorbed ^{18}O atoms as well as ^{18}O lattice atoms was also studied, and the TPD results are shown in Fig. 8. Consistent with ^{14}NO adsorption on a similar $^{16}O_2$-treated sample, $^{15}N^{16}O$ desorbed at 400 and 800 K, but not at 700 K. Unlike the TPD results after $^{15}N^{16}O$ adsorption on an $La_2^{16,18}O_3$ surface which had no net oxygen adsorption (Fig. 7), $^{15}N^{18}O$ desorbed not only from the low-temperature site but also from the 800 K site, and $^{16}O^{18}O$, $^{18}O_2$, and $^{16}O_2$ were also desorbed at 800 K.

After a He pretreatment at 973 K and cooling to 700 K, NO was admitted to the catalyst. N_2O was formed to a greater extent during the initial contact of NO at 700 K than at 300 K, but little N_2 was produced, and again this reaction ended quickly (11). TPD of NO was performed after purging the sample in He at 700 K for 10 min and cooling to 300 K in He, and a single broad NO peak between 600 to 900 K accompanied by a broad O_2 peak between 700 and 900 K (11). It is possible that the 700 and 800 K peaks observed earlier overlapped to give a single band. Exposure of this He-treated sample to NO at 700 K gave a noticeably larger NO desorption peak at 800 K compared to that for NO adsorption at 300 K after a He pretreatment.

NO adsorption in the presence of O_2 was also examined because of interest in catalytic NO reduction in excess O_2 and the argument that NO_2 is an active intermediate in the reaction mechanism. After a standard He or O_2 pretreatment, the La_2O_3 sample was introduced to a

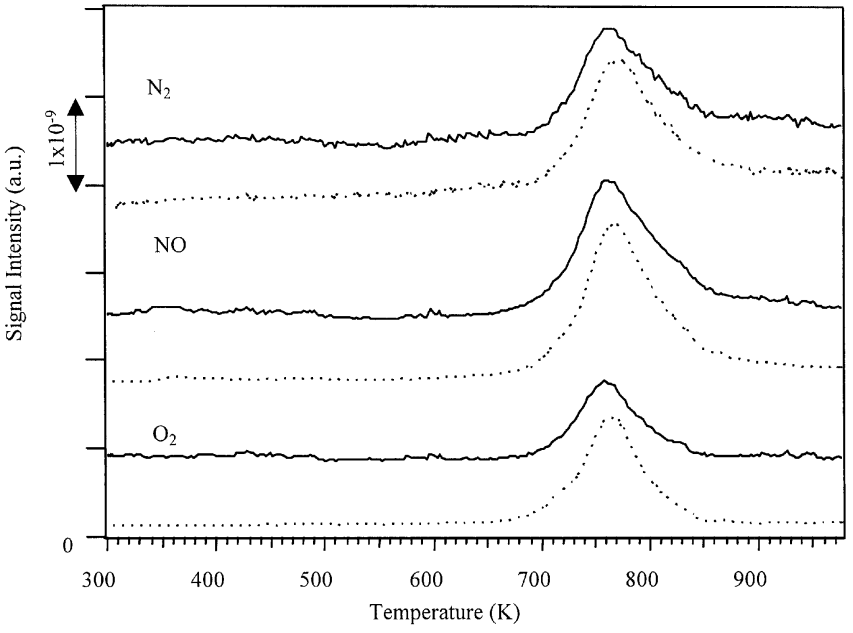

FIG. 9. TPD after NO + O_2 coadsorption on La_2O_3: solid line, He pretreatment, and dotted line, O_2 pretreatment.

stream containing 3.2% NO and 2.0% O_2 in He at 300 K. As shown in Fig. 9, TPD results were similar after either pretreatment. The low-temperature NO peak between 350 and 450 K is broad and extremely weak, while the high-temperature NO desorption peak is greatly enhanced and shifted 30 K lower than when only NO was present during adsorption. This may be due to higher coverage of the nitrate species (~50%) when exposure to both NO and O_2 at 300 K. A small amount of N_2 was also formed at the high-temperature site, but no NO_2 was detected during the entire TPD experiment. The respective amounts of NO, O_2, and N_2 desorbed during TPD are shown in Table 1.

The DRIFT spectra from La_2O_3 after various pretreatments, referenced to KBr powder at 300 K, are shown in Fig. 10. Only the sample given the initial calcination at 1023 K was exposed to air afterward (spectrum a); the other three were not air exposed. Fundamental La–O vibrations occurred at 940 and 920 cm^{-1} (5). Unidentate carbonate peaks at 848, 1070, 1370, and 1481 cm^{-1}, and bidentate carbonate peaks at 848, 1024, 1562, and 1309 cm^{-1}, were identified in all samples, in agreement with previous studies which have shown the stability of these surface (or subsurface) carbonates (8, 10). Nevertheless, the H_2 treatment seemed to be more effective in removing carbonates than the treatments in O_2 or Ar. A small peak at 3650 cm^{-1} representing isolated OH groups was present after each pretreatment (8, 10).

Figure 11 shows the IR spectra obtained after flowing NO over H_2-treated La_2O_3 at 300 K and referenced to the spectrum taken in Ar just before NO adsorption. After exposure of the sample to NO for 10 min, peaks appeared at 1604, 1579, 1354, 1300 (shoulder), 1243, 1179, 1119, 1093, 970, and 896 cm^{-1} and their intensity increased with exposure time except for those at 1579 and 1300 cm^{-1}, which disappeared, and the bands at 1093 and 1121 cm^{-1}, whose intensity decreased and tended to form a single peak after

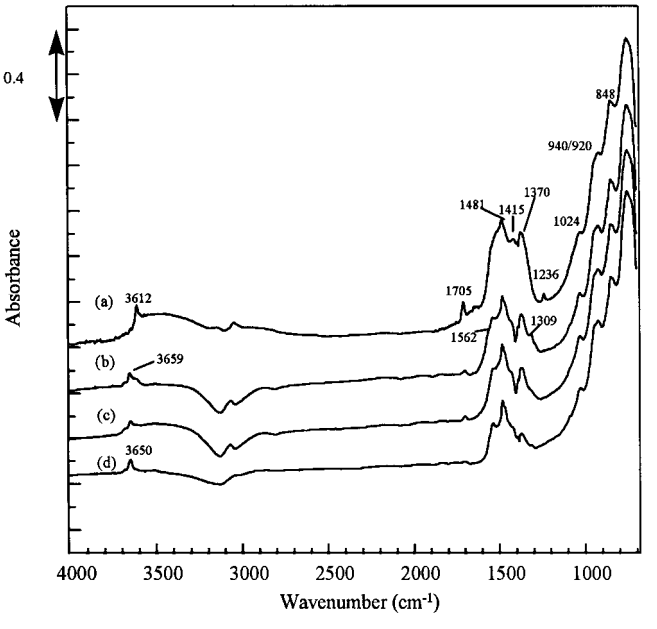

FIG. 10. DRIFT spectra of La_2O_3 after different pretreatments: (a) after calcination at 1023 K for 10 h and exposure to air during sample handling; (b) after *ex situ* treatment in He at 973 K for 1 h followed by *in situ* treatment in flowing Ar at 800 K for 1 h; (c) after *ex situ* treatment in He at 973 K for 1 h followed by *in situ* treatment in flowing O_2 at 800 K for 1 h; and (d) after *ex situ* treatment in He at 973 K for 1 h followed by *in situ* treatment in flowing H_2 for 0.5 h then 0.5 h in flowing Ar at 800 K. All spectra were taken at 300 K and referenced to KBr background at 300 K.

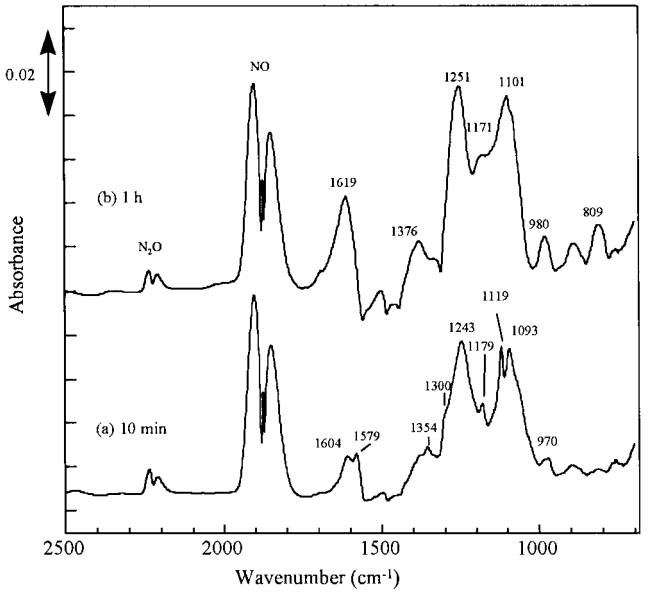

FIG. 11. DRIFT spectra after flowing 4% NO in Ar at 300 K through H_2-treated La_2O_3 for (a) 10 min and (b) 1 h.

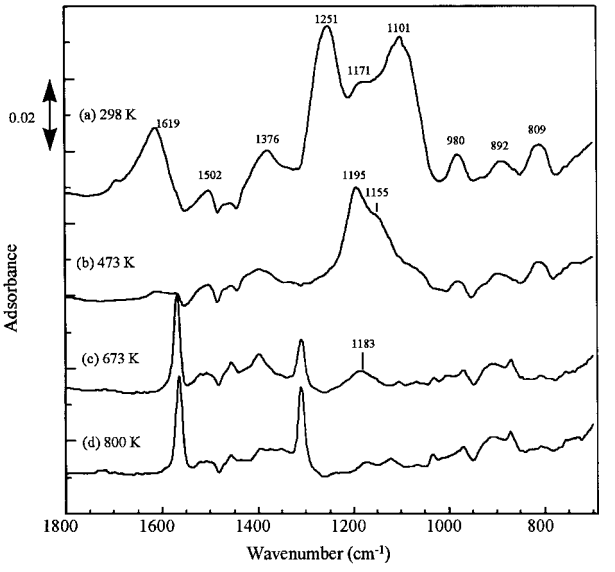

FIG. 12. DRIFT spectra after NO chemisorption at 300 K on H_2-treated La_2O_3 (a) after flowing 4% NO in Ar for 60 min at 300 K and purging in Ar for 30 min then heating in Ar to (b) 473 K, (c) 673 K, or (d) 800 K. All spectra were acquired after cooling of the sample to 300 K and are referenced to La_2O_3 just prior to the introduction of NO at 300 K.

exposure to NO for 1 h. Although H_2-treated La_2O_3 had fewer carbonate species than that treated in either Ar or O_2 (Fig. 10), overlap of NO_x bands with carbonate bands between 1300–1600 cm^{-1}, where they are most intense, was still unavoidable. Based on the spectra obtained after CO_2 adsorption on La_2O_3 as well as literature data, the peaks at 1579 and 1300 cm^{-1} can be assigned to bidentate carbonates (8, 12–14). To further resolve the thermal stability of the adsorbed species after NO adsorption at 300 K, this sample was heated under flowing Ar to progressively higher temperatures of 473, 673, and finally 800 K. After heating to 473 K, bands in the 1200–1100 cm^{-1} region were the most dominant feature (Fig. 12b), while after heating to 673 K only a weak broad band near at 1183 cm^{-1} remained; however, bands associated with bidentate carbonate species at 1575, 1310, and 871 cm^{-1} increased (Fig. 12c). Finally, after heating to 800 K, only bidentate carbonates could be identified. The two difference spectra shown in Fig. 13 were acquired by subtracting the spectrum after heating to 473 K from that at 298 K, and subtracting the spectrum after heating to 673 K from that after heating to 473 K, which mimics the TPD procedure. Thus, any positive peaks represent species that were not stable within the given temperature interval and were removed.

The species removed by heating the sample to 473 K, which have bands at 1612, 1254, and 983 cm^{-1}, appear to be bridging nitrate species on the oxide surface (15–18). Nitrito species (unidentate, M–O–N=O$^-$) have ranges of vibrational frequencies at 1485–1400 ($\nu\nu_{N=O}$), 1110–1050 ($\nu\nu_{NO}$), and 840–820 cm^{-1} ($\delta\delta_{ONO,\text{ bending ONO}}$) (15–17, 19, 20). If the nitrito group is chelated, the vibrational frequencies for these three bands are at 1390–1266 ($\nu\nu_{NO_2,assym}$), 1230–1170 ($\nu\nu_{NO_2,sym}$), and 900–850 cm^{-1} ($\delta\delta_{ONO}$) (15). Thus one can tentatively assign the bands at 1354 and 1171 cm^{-1} to chelated nitrites, while the band at 1098 cm^{-1} and the

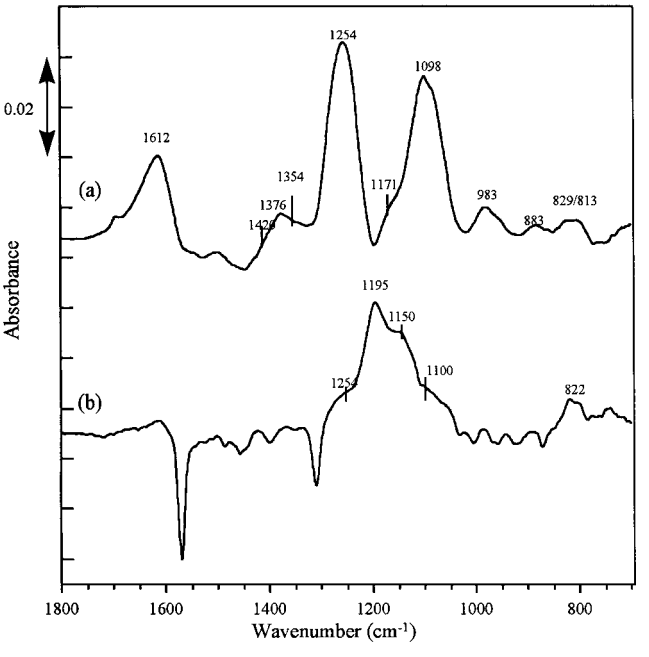

FIG. 13. Difference spectra obtained by subtraction of the spectrum from Fig. 14 after heating of the sample to higher temperature from that after heating to a lower temperature; thus positive peaks indicate species lost: (a) Fig. 14b subtracted from Fig. 14a; (b) Fig. 14c subtracted from Fig. 14b.

broad unresolved band around 813 cm^{-1} can be associated with the NO stretching and ONO bending frequencies of unidentate nitrito species, $M{-}O{-}N{=}O^-$. The band around 1485–1400 cm^{-1} for N=O stretching of the nitrito group ($\nu\nu_{N=O}$) cannot be resolved because of the negative peaks that appear in the same region due to the loss of carbonate species.

During heating from 473 to 673 K, bands at 1195, 1138 (shoulder), and 822 cm^{-1} started to decrease and they can be assigned to cis hyponitrite $(N_2O_2)^{2-}$ species and/or anionic nitrosyl NO^- species on the basis of the following spectroscopic evidence. The cis hyponitrite $(N_2O_2)^{2-}$ groups observed in the solid state exhibit IR bands at 1314 ($\nu\nu_{N=N}$), 1047 ($\nu\nu_{a,N-O}$), and 837 ($\nu\nu_{s,N-O}$) cm^{-1} in $Na_2N_2O_2$ (21, 22) and at 1304, 1057, and 857 in $K_2N_2O_2$, but the band at around 1300 cm^{-1} ($\nu\nu_{N=N}$) is very weak (23). The cis $N_2O_2^{2-}$ species on metal oxide surfaces has also been reported by Borello *et al.* to have vibrational frequencies at 1384, 1190, 1150, and 830 cm^{-1} on the basis of a study of NO adsorption on MgO (24), whereas for NO on CeO_2 these frequencies have been reported to be at 1350, 1015, and 954 cm^{-1} by Martinez-Arias *et al.* (25). The frequency for the N–O stretch vibration in nitrosyl species on metal oxides falls between 1000–2200 cm^{-1}, depending on the type of bonding on the surface (20, 24–29). If NO donates one electron and becomes a positive nitrosonium NO^+ ion, the N–O stretching frequency shifts from 1876 cm^{-1} (for gas-phase NO) to a higher value, whereas the formation of a nitrosyl NO^- anion, in which NO accepts an electron, results in a lower N–O frequency, i.e., a weaker N–O bond. Shelef and Kummer reported that purely ionic NO^- exhibits stretching frequencies between 1500–1700 cm^{-1} and the bond to the surface is mostly through the nitrogen end of the nitric oxide molecule (26). On the other hand, weaker N–O bonds in anionic NO^- species were observed on CaO (20), MgO (24), and reduced chromia (30) giving respective bands at 1100–1000, 1160, and 1305 cm^{-1}. As pointed out by Snis and Panas, the N–O distance and its stretching frequency depend on which end of the molecule interacts with the surface, and it appears from their quantum chemical calculations that monomeric NO^- with the O end down at an oxygen vacancy on a CaO surface displays a lower frequency than NO^- with the N end down (28). Although the calculated frequency of 1324 cm^{-1} for NO^- on CaO still exceeds the experimental values, lower frequencies can be obtained by increasing the charge donation into the antibonding π orbital of NO, and a calculated value of 981 cm^{-1} was achieved for an NO^{2-} species on CaO (28). In addition, NO adsorption on transition metals via the nitrogen atom is generally accepted, and the bonds involved are based on an interaction with metal *d*-electrons from the incomplete outer electron shell. It has been argued previously that the adsorption of NO on La cationic sites is not reasonable because the outer *d*-electron level of La^{3+} is empty and the required bonds cannot be formed, thus vacant anionic sites seem to be the optimum adsorption sites (5).

Although the bands in the spectra for different adsorbed NO_x species after NO adsorption at 298 K (Fig. 12a) can generally be resolved by the subsequent spectra taken after each heating sequence (Figs. 12b to 12d), the interference of carbonate bands in the latter three spectra is often worse than that in the former, thus it is desirable to verify these peak assignments by simulating the first spectrum, which contains the most adsorbed NO_x species, to see if the experimentally determined peak positions can be obtained. The peak fittings were performed between 1030–1300 cm^{-1} where the bands for NO_x species overlap the most. During the fitting process, the minimum number of peaks was used to obtain the best fit, and peak positions based on our own spectra were fixed, as explained previously, while three other parameters, i.e., amplitude, peak width, and peak shape for a Voigt function, were allowed to be optimized (5, 11). The sum of the squares of the deviations between experimental points and the fit values was minimized and was less than 10^{-4}, indicating that the quality of the fit was good and the peak assignments are reasonable. Examples of these spectra are available elsewhere (11).

With the Ar-treated sample, the admission of NO caused a significant loss of bidentate carbonate (bands at 1575, 1310, and 871 cm^{-1}), but this was complemented by a gain in unidentate carbonates at 1510 and 1350–1400 cm^{-1}, as shown in Fig. 14. These carbonate bands seriously interfered with those representing adsorbed NO_x species. An intense,

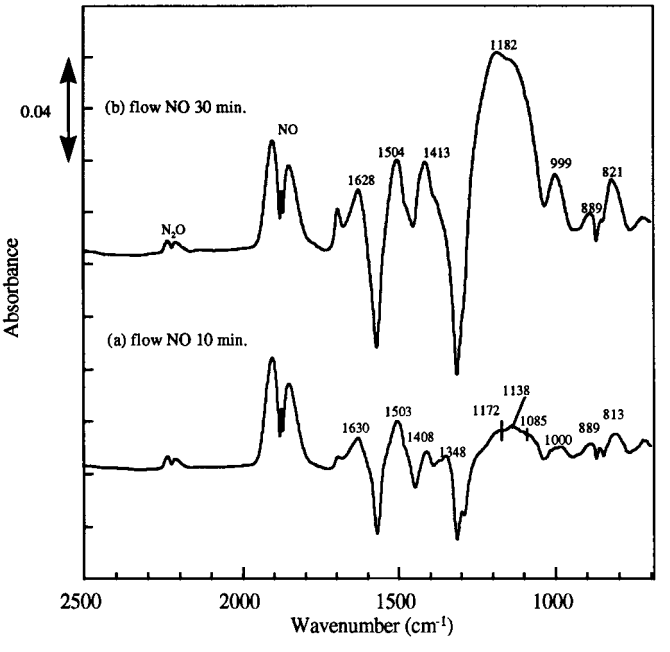

FIG. 14. DRIFT spectra after flowing 4% NO in Ar at 300 K over Ar-treated La_2O_3 for (a) 10 min and (b) 30 min.

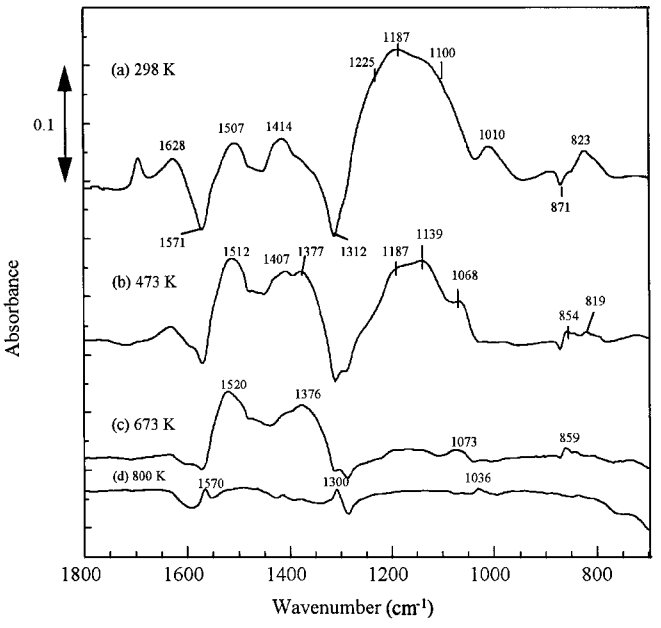

FIG. 15. DRIFT spectra after NO chemisorption at 300 K on Ar-treated La_2O_3 (a) after flowing 4% NO in Ar for 30 min at 300 K and purging in Ar for 30 min, then heating in Ar to (b) 473 K, (c) 673 K, or (d) 800 K. All spectra were acquired after cooling of the sample to 300 K and are referenced to La_2O_3 just prior to the introduction of NO at 300 K.

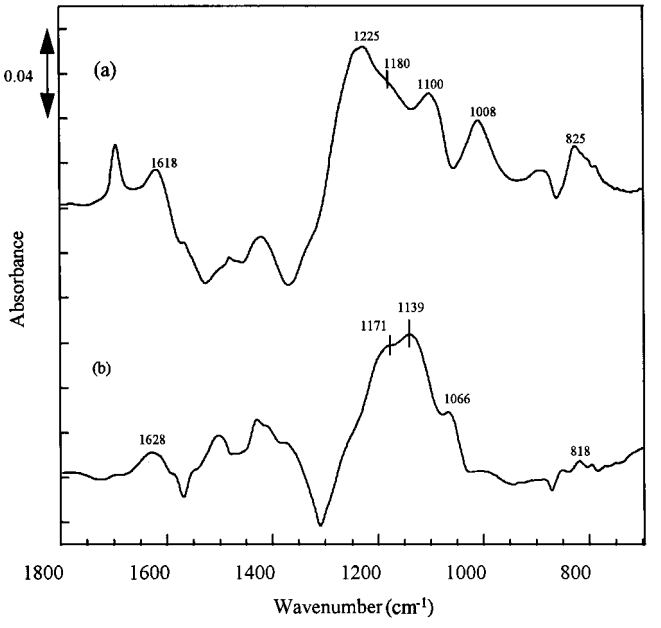

FIG. 16. Difference spectra obtained by subtraction of the spectrum from Fig. 17 after heating of the sample to higher temperature from that after heating to a lower temperature; thus positive peaks indicate species lost: (a) Fig. 17b subtracted from Fig. 17a; (b) Fig. 17c subtracted from Fig. 17b.

broad peak between 900–1300 cm^{-1} showing a maximum at 1182 cm^{-1} was observed after NO was flowed for 30 min over the Ar-treated La_2O_3 at 298 K. Figure 15 shows the effects of subsequent heating to higher temperatures. The changes in absorption band intensities during the heating sequences from 298 to 473 K and then up to 673 K are shown in Fig. 16, which again demonstrates that chelated nitrite, nitrito, and bridging nitrates were not stable during heating to 473 K, and the subsequent heating to 673 K caused the possible loss of NO^- and $N_2O_2^{2-}$ species.

The DRIFTS experiments with an O_2-treated La_2O_3 sample were originally intended to study the effects of chemisorbed oxygen on NO adsorption, as observed during TPD runs; however, due to the differences between the DRIFTS and TPD systems such that the *in situ* treatment in the IR cell cannot exceed 800 K, the DRIFT spectra obtained with an O_2-treated La_2O_3 sample after NO adsorption do not differ much from those acquired with an Ar-treated sample. Figure 17 shows the effect of exposure time as NO was flowed at 300 K over the O_2-treated sample. Bands at 1616, 1518, 1415, 1362, 1205, 1130 (shoulder), 1015, and 824 cm^{-1} were obtained after NO was flowed for 30 min. After adsorption, the sample was sequentially heated first to 473 K, then to 673 K, and finally to 800 K in Ar, and after cooling from each temperature to 300 K, separate DRIFT spectra were obtained, which are shown in Fig. 18. The interference due to the intensity loss for bidentate carbonates is not as severe as that with the Ar-treated sample (compare Figs. 17 and 14), and new bands representing unidentate nitrates (1518, 1265, and 1017 cm^{-1}) can now be distinguished in the spectra acquired after the sample was heated to 673 or 800 K (Fig. 18b or 18c). During the heating sequences, the carbonate levels did not remain constant at all temperatures; i.e., an increase in unidentate carbonates

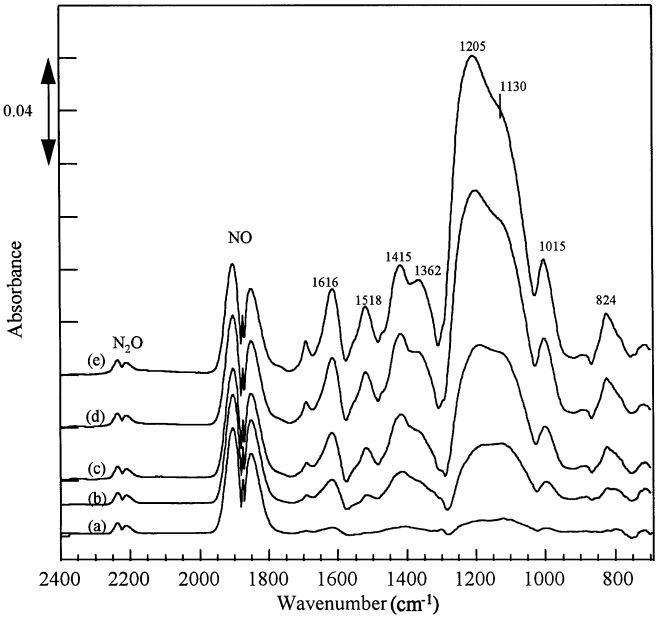

FIG. 17. DRIFT spectra after flowing 4% NO in Ar at 300 K over O_2-treated La_2O_3 for (a) 1 min, (b) 6 min, (c) 12 min, (d) 20 min, and (e) 30 min.

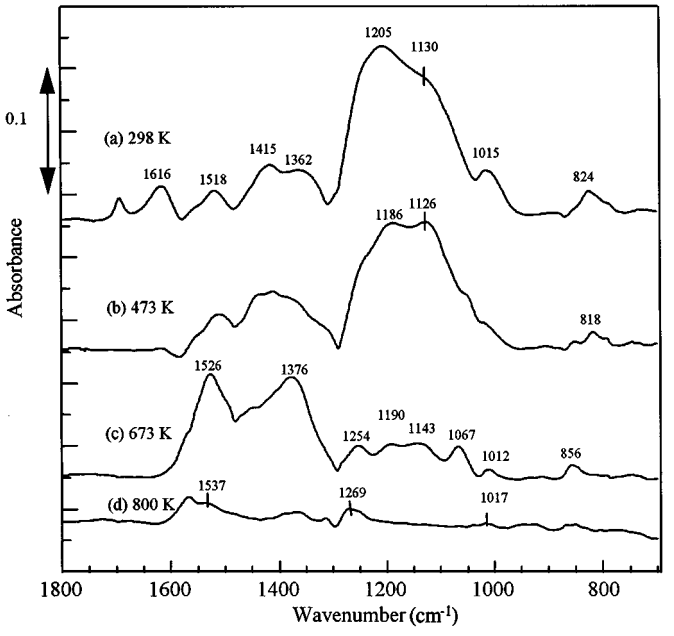

FIG. 18. DRIFT spectra after NO chemisorption at 300 K on O_2-treated La_2O_3 (a) after flowing 4% NO in Ar for 30 min at 300 K and purging in Ar for 30 min, then heating in Ar to (b) 473 K, (c) 673 K, or (d) 800 K. All spectra were acquired after cooling of the sample to 300 K and are referenced to La_2O_3 just prior to the introduction of NO at 300 K.

(represented by bands at 1526, 1376, 1067, and 856 cm^{-1}) was observed on the sample after heating to 673 K (Fig. 18b), but these carbonates were removed after subsequent heating to 800 K (Fig. 18c).

In situ IR spectra obtained under flowing NO at 473, 673, and 800 K, as well as spectra after a 10-min purge in Ar at each temperature, are shown in Fig. 19. At each temperature, a broad peak between 1000–1300 cm^{-1}, consisting of bands for NO^- (1000–1200 cm^{-1}), $(N_2O_2)^{2-}$ (1100–1200 cm^{-1}), and unidentate nitrate (1015, 1265 cm^{-1}), dominates in the presence of gas-phase NO. After a purge in Ar, the intensity of this feature remained almost unchanged at 473 K, but decreased at 673 K and finally disappeared at 800 K except for a small residual band at 1260 cm^{-1}. Although NO^- and $(N_2O_2)^{2-}$ desorb in Ar at temperatures above 473 K, they still exist in significant amounts when gas-phase NO is present. The N_2O observed at all temperatures (2224 cm^{-1}) comes from the impurity in the NO gas cylinder although a small contribution from the NO reaction is also possible. At 473 K, a small peak at 2170 cm^{-1} was also observed during exposure to NO. Although it is near the band position for gas-phase N_2O, it is unlikely to be due to any adsorbed N_2O species because flowing N_2O over the catalyst at this temperature did not produce a 2170 cm^{-1} peak (not shown) (11). It is more likely to be a C=N vibrational frequency resulting from an NCO or a CN species formed by an interaction between NO and carbonate groups on the La_2O_3 surface (15).

The adsorption of NO on an Ar-treated La_2O_3 sample in the presence of O_2 was conducted using 2.0% NO and 2.4% O_2 in Ar at either 300 or 800 K. The gas-phase composition is complex because NO can homogeneously react with O_2 to form NO_2, and NO_2 can then dimerize in the gas phase to form N_2O_4, i.e.,

$$2NO + O_2 \rightleftharpoons 2NO_2 \quad [1]$$

$$2NO_2 \rightleftharpoons N_2O_4. \quad [2]$$

Both are reversible reactions in which thermodynamic equilibrium shifts to the right at lower temperatures (29). After this $NO + O_2$ mixture was flowed over La_2O_3 for 10 min at 300 K, peaks at 1876 cm^{-1} for gas-phase NO and 1617 cm^{-1} (doublet, $\nu\nu_{as}$) for $NO_{2(g)}$ can be identified as well as intense absorption bands below 1650 cm^{-1} signifying adsorbed NO_x species, as shown in Fig. 20a. Gas-phase N_2O_4 absorbing at 1753 and 1264 cm^{-1} was also present but the latter peak is superimposed with absorption frequencies due to adsorbed NO_x species. A subsequent purge in Ar at 300 K (Fig. 20b) removes the peaks for the gas-phase molecules but does not change the features of the adsorbed NO_x species, as compared to Fig. 20a. At 800 K, only peaks for gas-phase NO and NO_2 along with bands at 1544, 1262, and 1007 cm^{-1} were observed during exposure to $NO + O_2$ (Fig. 20c) and, after a purge in Ar, the latter three bands were still present, although their intensities were decreased (Fig. 20d).

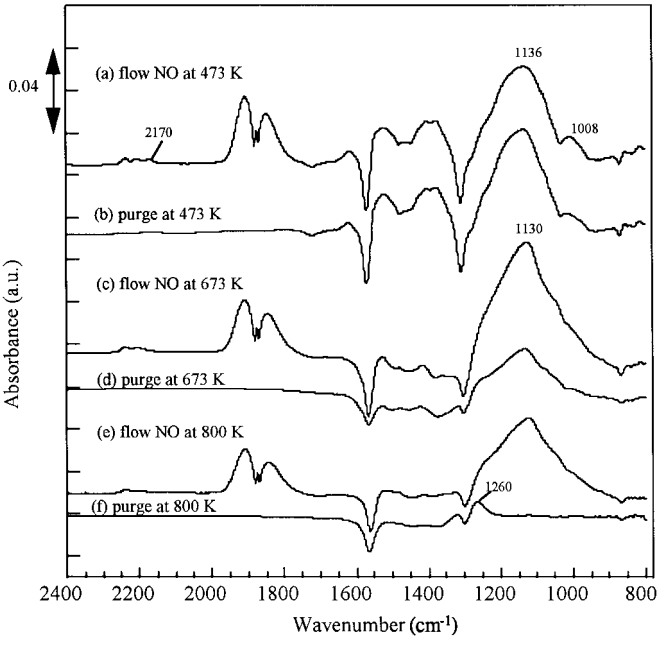

FIG. 19. DRIFT spectra after flowing NO at 473 K, 673 K, and 800 K for 30 min followed by purging in Ar at each respective temperature for 10 min. Spectra were referenced to the La_2O_3 sample in Ar at each respective temperature before NO was introduced.

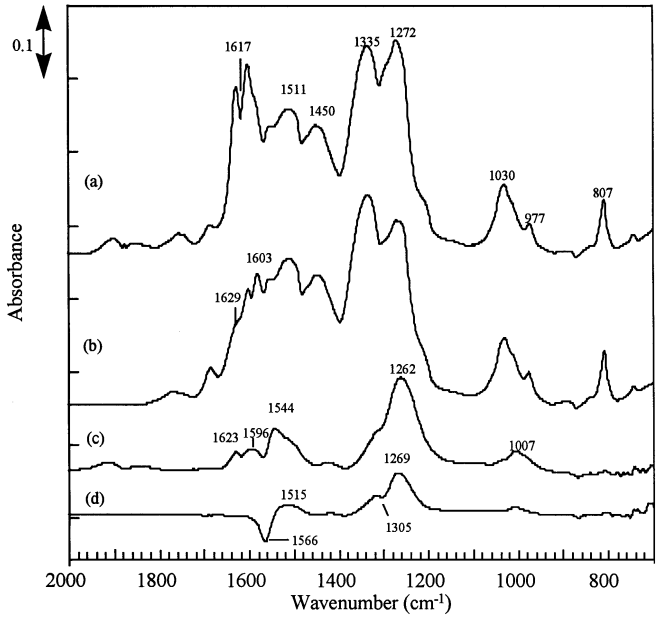

FIG. 20. DRIFT spectra after flowing NO + O_2 at 300 and 800 K for 30 min (spectra a and c) followed by purging in Ar at each respective temperature for 5 min (spectra b and d). Spectra were referenced to the La_2O_3 sample in Ar at each respective temperature just prior to the introduction of NO + O_2.

Free NO^{2-} ions have been reported to absorb at 1250 ($\nu\nu_{NO_2,as}$) and 1335 ($\nu\nu_{NO_2,s}$) cm^{-1}, and nitro species in the form of M–NO_2 have vibrational frequencies at 1370–1470, 1320–1340, and 820–840 cm^{-1} (15). At 300 K, the adsorbed species formed were identified as bidentate nitrates (1603, 1260 cm^{-1}, superimposed with other bands), unidentate nitrates (1511, 1260, 1030 cm^{-1}), free NO^{2-} ions (1250, 1335 cm^{-1}), and nitro M–NO_2 species (1447, 1334, and 807 cm^{-1}). At 800 K, the unidentate nitrates were the most dominant species. All the absorption bands observed on La_2O_3 after exposure to either NO or NO + O_2 mixtures are illustrated in Table 2.

DISCUSSION

A previous study of O_2 chemisorption on La_2O_3 after a He pretreatment showed that both reversible and irreversible adsorption at 300 K was negligible but the oxygen adsorption capacity increased with temperature and reached a maximum at 573 K, with an irreversible uptake of 0.2 μmol/m^2 and a total uptake of 1.1 μmol/m^2, then declined (3). Our present study is consistent with these results in that no O_2 TPD peak was observed after exposure to O_2 at either 300 or 500 K, and 1.0 μmol/m^2 of desorbed O_2 was calculated from the TPD spectrum after exposure to O_2 during cooling from 973 to 300 K. In addition, when $^{18}O_2$ adsorbed, $^{16}O_2$, $^{16}O^{18}O$, and $^{18}O_2$ were found to desorb during TPD, thus indicating that O_2 chemisorption is dissociative as well as activated (because this occurred after exposure from 973 to 300 K but not after exposure of O_2 at 500 or 300 K.)

Several forms of oxygen species have been reported on metal oxide systems. ESR spectra have allowed the identification of O^-, O_2^-, and O_3^- species on Li/MgO (31) and O_2^- on La_2O_3 (32, 33). In the latter case, O_2^- species were formed on La_2O_3 after calcination at 823 K in 600 Torr O_2 for 1 h and cooling to 77 K in the presence of O_2. This species can also be formed at room temperature by adsorbing O_2 on La_2O_3 after treatment of the surface in a vacuum at 823 K for 1 h (33). O_2^{2-} species have been detected on Ba/La_2O_3 and Ba/MgO by XPS after treatment of the surface in O_2 at 1073 K and cooling in O_2 to 300 K (34, 35). The chemisorption of O_2 on oxygen-ion-conducting solids occurs on oxygen defect sites and can result in a variety of oxygen species on the surface (36–38), and Sokolovskii has mentioned that all these oxygen species might exist in equilibrium depending upon the nature of the catalyst (36), i.e.,

$$O_{2(g)} \rightleftharpoons O_{2(ad)} \overset{+e^-}{\rightleftharpoons} O_2^- \overset{+e^-}{\rightleftharpoons} O_2^{2-} \rightleftharpoons 2O^- \overset{+2e^-}{\rightleftharpoons} 2O^{2-}. \quad [3]$$

Although O^- and O_2^{2-} have not been detected on La_2O_3, these species have been modeled by computer simulation techniques and these calculations indicate that the {011} surface favors the creation of O_2^{2-} peroxide species, which can be regarded as a dimer of the O^- species (39). Our TPD results show no O_2 desorption peak after exposure to O_2 at 300 K. Since the O_2 desorption peak at 620 K (Fig. 1) cannot be due to O_2 adsorbed at room temperature, it is not likely to be from an O_2^- species. Although O_2^- species have been observed at 823 K in the presence of gas-phase O_2, they are not stable at elevated temperatures in vacuum or under flowing He or CH_4 (33).

The nature of adsorbed oxygen species on La_2O_3, especially those active in catalytic reactions involving NO and CH_4, is still being debated. Winter proposed that the O_2 adsorption/desorption process involves pairs of associated F^+ centers (oxygen vacancies with one trapped electron) or a so-called R_2 center (40, 41), i.e.,

$$2(O^-|\square) \rightleftharpoons (e^-|\square)(e^-|\square) + O_{2(g)} \quad [4]$$

where, for simplicity, $\square$ represents an anion vacancy with or without a trapped electron. At elevated temperatures, R_2 centers can be formed via Eq. [4] and destroyed by either O_2 chemisorption (reverse of Eq. [4]) or migration of neighboring O^{2-} ions according to Eq. [5]:

$$(e^-|\square)_1(e^-|\square)_2 + (O^{2-}|\square)_3 \rightleftharpoons (O^{2-}|\square)_1 + (e^-|\square)_2 + (e^-|\square)_3, \quad [5]$$

where the subscripts refer to the three sites concerned. The reaction mechanism for oxygen exchange was proposed by

TABLE 2

Reported Frequencies of Adsorbed NO_x Species Observed on Metal Oxides and Their Corresponding Structure

NO_x species	Structure	Vibration	Inorganic compound or metal oxide (13, 16–27)	La_2O_3 (this study)
Free nitrite ion, NO_2^-		$\nu\nu_{(NO_2,as)}$	1250	
		$\nu\nu_{(NO_2,s)}$	1335	
		$\delta\delta_{ONO}$	830	
Nitro		$\nu\nu_{(NO_2,as)}$	1370–1470	
		$\nu\nu_{(NO_2,s)}$	1320–1340	
		$\delta\delta_{ONO}$	820–850	
Nitrito		$\nu\nu_{(N=O)}$	1400–1485	1420
		$\nu\nu_{(NO)}$	1050–1100	1083
		$\delta\delta_{ONO}$	820–840	830
Chelated nitrite		$\nu\nu_{(NO_2,as)}$	1270–1390	1340
		$\nu\nu_{(NO_2,s)}$	1170–1225	1171
		$\delta\delta_{ONO}$	840–860	830
Bridging nitro		$\nu\nu_{(NO_2,as)}$	1390–1520	
		$\nu\nu_{(NO_2,s)}$	1180–1260	
Free nitrate ion, NO_3^-		$\nu\nu_{(NO_2,as)}$	1430	
Unidentate nitrate		$\nu\nu_{(NO_2,as)}$	1450–1570	1518
		$\nu\nu_{(NO_2,s)}$	1250–1330	1265
		$\nu\nu_{(NO)}$	970–1035	1015
Bidentate nitrate		$\nu\nu_{(NO_2,as)}$	1200–1310	
		$\nu\nu_{(N=O)}$	1500–1620	
		$\nu\nu_{(NO_2,s)}$	1003–1040	
Bridged nitrate		$\nu\nu_{(NO_2,as)}$	1200–1260	1240/1254
		$\nu\nu_{(N=O)}$	1590–1660	1607/1616
		$\nu\nu_{(NO_2,s)}$	1000–1030	998
Nitrosyl, NO^-	*M*–ON^- or *M*–NO^-	$\nu\nu_{(NO)}$	1810–1103	1195
Cis hyponitrite ion		$\nu\nu_{(N-N)}$	1304/1314	
		$\nu\nu_{(NO,s)}$	1042–1057	1138
		$\nu\nu_{(NOas)}$	830–857 [from NaN_2O_2 (18)]	822
		$\nu\nu_{(N-N)}$	1384	
		$\nu\nu_{(NO,s)}$	1190	
		$\nu\nu_{(NOas)}$	1150	
		$\delta\delta_{(NNO)}$	830 [NO on MgO (15)]	

Winter to be composed of chemisorption of $^{18}O_2$, as shown in Eq. [4], followed by migration of $(^{18}O^-|\square)$ species via charge exchange with a lattice O^{-2} ion (40):

$$(^{18}O^-|\square)_1 + (^{16}O^{2-}|\square)_2 \rightleftharpoons (^{18}O^{2-}|\square)_1 + (^{16}O^-|\square)_2. \quad [6]$$

Desorption of the exchanged product occurs after a random interaction of two $(O^-|\square)$ species. Unfortunately, no experimental evidence has been presented for F^+ centers or R_2 centers on La_2O_3; however, point defects such as F^+ or F centers (representing an oxygen vacancy which has captured one or two electrons) are quite common in rock salt oxides, such as MgO, CaO, and SrO (42).

Instead of the assumption of the existence of R_2 centers, Lacombe *et al.* have proposed the activation of O_2 via a pair of sites containing a coordinatively unsaturated oxygen ion coupled with an oxygen vacancy, i.e., $\{O^{2-}_{cus} + \square\}$ (43). The mechanism for isotopic O_2 exchange can then be written in the following way,

$$\begin{aligned} {}^{18}O_{2(g)} + 2\{{}^{16}O^{2-}_{cus} + \square\} &\rightleftharpoons 2\{{}^{16}O^-, {}^{18}O^-\} \\ &\rightleftharpoons \{{}^{16}O\,{}^{18}O_{(g)} + \{{}^{16}O^{2-}_{cus} + \square\} + \{{}^{18}O^{2-}_{cus} + \square\} \quad [7] \end{aligned}$$

and

$$\{{}^{18}O^{2-}_{cus} + \square\} + {}^{16}O^{2-}_{l} \rightleftharpoons \{{}^{16}O^{2-}_{cus} + \square\} + {}^{18}O^{2-}_{l}, \quad [8]$$

where O^{2-}_{l} represents a bulk lattice anion. They also

observed from temporal analysis of products (TAP) experiments that the exchange process at 1023 K with La_2O_3 mixes all the oxygen atoms of the oxide via the reversible step [8]. Kalenik and Wolf also studied the oxygen exchange reaction by exposing La_2O_3 to a step change of $^{18}O_2$ in He at 1023 K for a period of 7 min, and they showed that this procedure was sufficient to achieve 80% exchange between the isotopic and unlabeled lattice oxygen (44).

In our study, pulsed oxygen exchange was performed with La_2O_3 at 500 K after one of the three pretreatments. La_2O_3 after the He pretreatment showed the highest exchange rate, while saturation of the surface sites with O_2 by cooling from 973 to 500 K reduced the exchange ability. This may be due to the creation of oxygen vacancies at 973 K, i.e.,

$$2O_l^{2-} \rightarrow O_{2(g)} + (2e^-|\square)(2e^-|\square), \qquad [9]$$

where $(2e^-|\square)$ represents an oxygen vacancy with two trapped electrons. It is known that La_2O_3 is an *n*-type semiconductor in an O_2-deficient atmosphere and a *p*-type semiconductor under oxidation conditions (37, 45, 46). For example, at 1305 K the total conductivity of La_2O_3 increases with P_{O_2} when $P_{O_2} > 10^{-9}$ atm (*p*-type), it decreases with P_{O_2} when $P_{O_2} < 10^{-12}$ atm (*n*-type), and it is independent of P_{O_2} when the oxygen partial pressure is between these limits, thus indicating the mobility of lattice oxygen atoms (46). At high temperatures, one or both of the localized (trapped) electrons can be excited to the conduction band and transferred away from the oxygen vacancy, which then becomes either singly or doubly ionized, and the distribution of the three differently charged oxygen vacancies is equilibrated:

$$(2e^-|\square) \rightleftharpoons (e^-|\square) + e^-_{cond} \rightleftharpoons \square^0 + 2e^-_{cond}. \qquad [10]$$

No observable conductivity has been reported near 300 K for low-surface-area La_2O_3 (46–49) and the forbidden band gap is wide, with literature data varying from 2.8 to 5.4 eV (46, 50), indicating that the electrons are mainly localized at low temperatures, but their locations are not clear. They may be trapped at either the normal cation sites or the anion vacancies in the bulk; however, the former is unlikely because La_2O_3 (La^{3+}) is generally considered to be nonreducible although some reports suggest that the surface of lanthana may be reducible (6). On the other hand, the doubly charged oxygen defects in the bulk can be generated through a Frenkel disorder, where an oxygen anion is transferred to an interstitial position, but the defect concentration will be very low in the undoped material (51). The formation of pair vacancies created by O_2 desorption at high temperature, as indicated by Eqs. [4] and [9], is also competing with the diffusion rate of vacancies through bulk La_2O_3 and the surface rearrangement to form two single vacancies due to the migration of surface oxygen ions. Therefore, at a given temperature and oxygen partial pressure, a certain equilibrium distribution of oxygen single vacancies and pair vacancies is present, although the distribution may not always be maintained because the cooling process was not controlled. The exposure of the surface to NO prior to the exchange reaction at 500 K completely blocked the exchange sites, clearly indicating that NO adsorption at 500 K is associated with oxygen vacancy sites.

Our TPD study of La_2O_3 demonstrates that the adsorption behavior of NO is affected by the catalyst pretreatment. Three NO desorption peaks at ca. 400, 700, and 800 K were found after He pretreatment, but only two peaks at 400 and 800 K were obtained following an O_2 pretreatment. In either case NO and O_2 desorption at 800 K occurred simultaneously and their intensities were enhanced by the O_2 pretreatment. The effect of either lattice oxygen or chemisorbed oxygen on NO adsorption was investigated by ^{15}NO adsorption on an ^{18}O-exchanged La_2O_3 surface with and without chemisorbed ^{18}O atoms. When $^{15}N^{16}O$ was adsorbed on $La_2{}^{16,18}O_3(^{16,18}O)$, both $^{15}N^{16}O$ and $^{15}N^{18}O$ were found in the desorption peaks at 400 and 800 K, and $^{16}O_2$, $^{16}O^{18}O$, and $^{18}O_2$ were desorbed at 800 K (Figure 8); however, $^{15}N^{18}O$ desorbed only at 400 K from an $La_2{}^{16,18}O_3$ surface containing only lattice-exchanged ^{18}O (Fig. 7). Consequently, the following conclusions can be reached. (a) The 400 K NO desorption site involves interaction with the lattice oxygen. (b) The 800 K NO desorption site is associated with only chemisorbed oxygen because if this adsorption site allowed interaction with lattice O, then $^{15}N^{18}O$ should be desorbed at 800 K from an exchanged $La_2{}^{16,18}O_3$ surface without chemisorbed oxygen. (c) The NO species desorbed at 700 K is not bound with either lattice O or chemisorbed O atoms because no exchanged $^{15}N^{18}O$ was observed. (d) The 700 K NO desorption sites are the same as those for O_2 adsorption. The results gained only from the isotopic TPD studies cannot fully explain why NO and O_2 desorbed at 800 K from He-treated La_2O_3, which should have no chemisorbed oxygen prior to NO adsorption; however, this can be explained by the chemisorbed O that was formed during the disproportionation reaction between two NO molecules when La_2O_3 was first exposed to NO, because N_2O desorbs from the surface and an adsorbed O atom is left.

To clarify the mechanism of NO adsorption and desorption using the TPD results, the surface properties after each pretreatment and the character of the three NO desorption peaks must be taken into account. After the He pretreatment, there should be a certain distribution of oxygen pair vacancies, $(\square)_1(\square)_2$, and single vacancies, $(\square)$, coexisting on the surface. These vacancy sites would preferably be created at the tetrahedral $O_{(t)}$ position according to Ilett and Islam (51). When NO is admitted to the system, molecular NO adsorbs on the oxygen pair vacancy sites to produce N_2O, a chemisorbed oxygen atom, and a single vacancy, for

example:

$$2NO + (e^-|\square)_1(e^-|\square)_2 \rightleftharpoons (NO^-_{ad}|\square)_1(NO^-_{ad}|\square)_2 \rightleftharpoons (N_2O|\square)_1\left(O^{2-}_{ad}|\square\right)_2 \rightarrow (\square)_1\left(O^{2-}_{ad}|\square\right)_2 + N_2O_{(g)} \quad [11]$$

and

$$(\square)_1\left(O^{2-}_{ad}|\square\right)_2 \rightleftharpoons (e^-|\square)_1(O^-_{ad}|\square)_2 \quad [12]$$

This disproportion reaction between two adjacent adsorbed NO molecules ends after the vacancy pair sites are destroyed. N_2O formation at room temperature has also been observed after NO adsorption on other oxides such as Cr_2O_3 (52) and Mn_2O_3 (53).

To interpret the surface chemistry associated with NO adsorption on La_2O_3, the results from both TPD and DRIFTS experiments must be taken into account. Adsorption of NO on metal oxides often results in nitrite (NO_2^-) or nitrate (NO_3^-) species due to the interaction between NO and surface oxygen anions. As pointed out by Davydov and Rochester, the isolation of nitrate or nitrite compounds with a definite structure for interpretation of their spectra is largely symbolic because the difference in the structure of nitrate or nitrite surface compounds reflects primarily the difference in properties of the surface oxygen that participates in the formation of these structures (16). The absorption frequencies for the nitrate or nitrite species generally fall between 1700–800 cm^{-1}. On transition metal oxides, NO is also readily adsorbed on metal cations via the nitrogen end of the molecule, resulting in the formation of mononitrosyl (either M–NO^+, M–NO^-, or M–NO) or dinitrosyl or dimerized species, i.e., M–$(NO)_2$ (16–20, 26, 27, 30, 54–58). In the case of adsorbed mononitrosyl species, the bond strength for the positively charged NO^+ ion increases, thus giving a higher vibrational frequency (1876–2400 cm^{-1}) than that of the gas-phase NO molecule (1876 cm^{-1}). The N–O bond is weakened by the acquisition of an electron to form a negative ion having a vibrational frequency from 1500 to 1800 cm^{-1}. The bond strength is slightly weakened when NO is bonded covalently or purely coordinatively to the cations and give bands from 1700 to 1870 cm^{-1} (16, 26, 27, 55). The vibrational frequencies for the dinitrosyl complex exhibit a doublet between 1750–1900 cm^{-1} for the antisymmetric and symmetric vibrations (17–19, 57).

On the other hand, when NO is adsorbed on alkaline earth metal oxides such as MgO and CaO, in addition to nitrite and nitrate species, the negatively charged nitrosyl ion, NO^-, and the dimeric hyponitrite ion, $(N_2O_2)^{2-}$, are also observed (20, 24, 59, 60). In these cases, the bond strength of the N–O stretch is noticeably weakened, generating frequencies below 1500 cm^{-1}. The DRIFT spectra obtained in this study after NO adsorption on La_2O_3 show numerous bands in the range of 1700–800 cm^{-1} and no major band was found higher than 1700 cm^{-1}, indicating bonds for adsorbed NO species on La_2O_3 that differ from those of mononitrosyl or dinitrosyl species on transition metal oxides. Adsorption of NO on La_2O_3, therefore, is more likely to form nitrite and nitrate species as well as the NO^- and $(N_2O_2)^{2-}$ species that bond similarly to those on MgO or CaO surfaces. Literature values for the vibrational frequencies of these various surface species are summarized in Table 2 along with assignments for adsorbed species on La_2O_3 based on this study. On the basis of results reported here, the thermal stabilities of these species are in the following order: linear nitrites $\approx$ chelated nitrites $\approx$ bidentate or bridging nitrates $<$ NO^- ions $\approx$ hyponitrite species $<$ unidentate nitrates. It is then reasonable to propose that nitrite and bidentate/bridging nitrate species form at the 400 K NO desorption site. The chelated nitro group can be created by NO adsorbing at an oxygen single vacancy and interacting with a surface lattice oxygen, i.e.,

$NO + \{e^-|\square, O_l\} \rightarrow$ 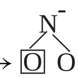 [13]

The bidentate or bridging nitrate species are formed via NO coordinating with two adjacent lattice oxygen atoms, which may contribute to the exchanged $N^{18}O$ observed during decomposition. The NO peak at 700 K may be assigned to the desorption of NO^- or hyponitrite $(N_2O_2)^{2-}$ species, which may be formed by NO adsorption on a single oxygen vacancy or on a vacancy pair site, respectively. The N_2O formed during NO adsorption at 300 K and the $(N_2O_2)^{2-}$ species assigned to the NO TPD peak at 700 K suggest that two types of surface oxygen vacancy pair sites exist, presumably with a different $\square$–$\square$ separation. Meanwhile, because of the location of the vacancies and their surroundings, there can be different types of surface oxygen single vacancies; consequently, one kind of single vacancy is responsible for the formation of nitrite species, as shown in Eqs. [11] and [12], and another kind allows for the NO^- species to be formed. This assignment for the NO desorption peak at 700 K is consistent with the results that no exchanged $N^{18}O$ was seen at 700 K in the isotopic TPD studies and no TPD peak for NO was observed at 700 K with La_2O_3 after an O_2 pretreatment because the oxygen vacancy sites were filled by chemisorbed oxygen. Finally, the NO TPD peak at 800 K is assigned to the decomposition of unidentate nitrate species because NO and O_2 desorptions were concomitant at this temperature and the NO/O_2 ratio was always about unity. The formation of the unidentate nitrate species can be illustrated by the NO adsorption on a pair vacancy sites occupied by two chemisorbed oxygen atoms, i.e.,

$(O^-_{ad}|\square)_1(O^-_{ad}|\square)_2 + NO \rightarrow$ 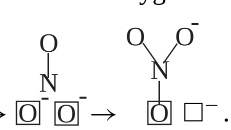 [14]

However, a comparison of the amount of O_2 desorbed at

800 K during NO TPD (3.1 μmol/m^2) to that desorbed during O_2 TPD (1.0 μmol/m^2) shows the former is noticeably larger. This indicates that not only chemisorbed O atoms but also some of the lattice oxygen atoms at the surface, which may have been activated by the treatment in O_2, contribute to the formation of unidentate nitrate species. During the O_2 pretreatment at high temperature, oxygen adsorption may also activate a neighboring lattice O^{2-} atom (40, 61), i.e.,

$$O_2 + 2O_{lat}^{2-} + 4\square \rightleftharpoons 4(O_{ad}^{-}|\square). \qquad [15]$$

A model of the La_2O_3 surface illustrating the different surface sites is shown in Fig. 21 for a surface after a pretreatment in He. Although desorption of O_2 at higher temperatures facilitates the formation of oxygen pair vacancies, these anion pair vacancies can convert to single vacancies due to the high mobility of lattice oxygen atoms, especially at the surface; therefore, a certain distribution of oxygen single and pair vacancies formed at elevated temperatures can remain when the surface is cooled to 300 K. To interpret the complex interaction between NO molecules and La_2O_3, several types of defects sites such as oxygen vacancies and low-coordination lattice oxygen atoms are considered. The

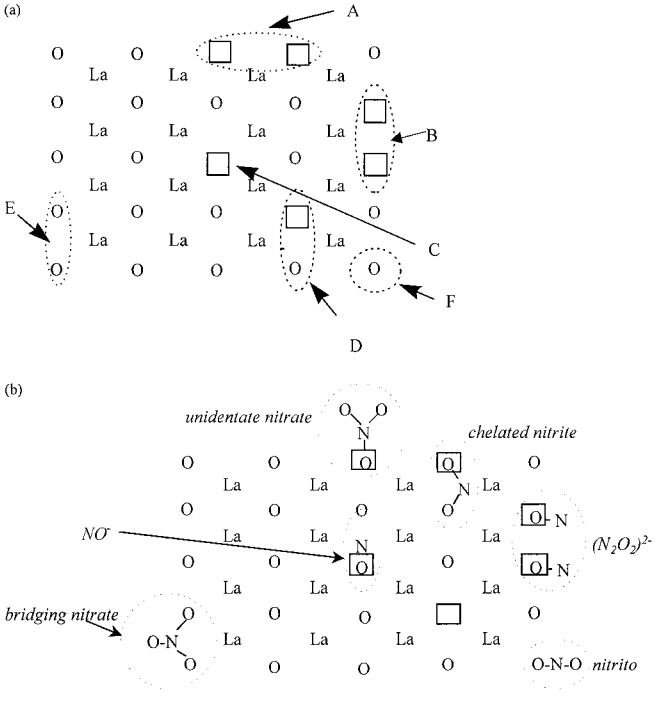

FIG. 21. (a) Model of La_2O_3 surface after He treatment at 973 K for 1 h: (A) oxygen pair vacancy type I ($e^-|\square$)($e^-|\square$) with an O–O distance of 397 Å; (B) oxygen pair vacancy type II ($e^-|\square$)($e^-|\square$) with a shorter O–O distance of 2.88 Å; (C) single oxygen vacancy, ($e^-|\square$); (D) single vacancy plus adjacent surface lattice oxygen atom, {$e^-|\square$,O_{lat}^{2-}}; (E) adjacent lattice oxygen atoms, {O_{lat}^{2-}, O_{lat}^{2-}} and (F) coordinative unsaturated lattice oxygen atom at corner site, O_{cus}^{2-}. (b) Proposed assignment of surface NO_x species to surface sites.

stoichiometric reaction to form N_2O during NO adsorption at 300 K and the presence of $(N_2O_2)^{2-}$ species detected by DRIFTS suggest that two types of oxygen pair vacancy sites exist, as depicted by site A and site B in Fig. 21a. On the basis of their location and surroundings, two types of single vacancies can exist: one is isolated with no interaction with any neighboring oxygen atoms (site C) and the other type is associated with a nearby lattice oxygen atom (site D). Adjacent lattice oxygen atoms (site E) and a coordinatively unsaturated surface oxygen site located at a corner (site F) are also shown.

We propose that, when NO is introduced onto the surface, two NO molecules adsorb on an oxygen pair vacancy (site A) to produce gas-phase N_2O and leave one oxygen atom chemisorbed on the surface at one of the vacancies. The interactions of NO with the different adsorption sites to form the IR-active species are represented in Fig. 21b. Nitrosyl anions, NO^-, and *cis* hyponitrite ions, $(N_2O_2)^{2-}$, are formed via NO adsorption on single oxygen vacancies (site C) and oxygen pair vacancies (site B), respectively. The formation of chelated nitrite ions,  , can be pictured as NO molecules adsorbed on D sites, which consist of a single oxygen vacancy associated with a neighboring lattice oxygen atom. Bridging nitrates,  , can be formed by NO interacting with two adjacent lattice oxygen atoms (site E). When NO is adsorbed on a coordinatively unsaturated (cus) oxygen atom (site F), nitrito species, M–O–N=O$^-$, can be formed. Finally, chemisorbed oxygen atoms, generated during N_2O formation at 300 K by consecutive reoxidation steps via Eqs. [11] and [12], can interact with NO to form unidentate nitrate species:

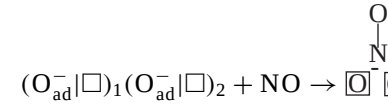

[16]

Chemisorption of oxygen at high temperature before NO adsorption fills the pair vacancy sites (sites A and B); consequently, this would facilitate the formation of unidentate nitrate but inhibit the formation of N_2O at 300 K and the formation of $(N_2O_2)^{2-}$ species (the 700 K TPD peak). However, some oxygen single vacancies (sites C and D) could still remain unfilled, thus providing sites for NO adsorption. Finally, it must be remembered that exchange between lattice and chemisorbed oxygen atoms can occur, as shown by Eqs. [7] and [8].

Keeping the previous description in mind, the actual configuration and surface structure of La_2O_3, which has a type A (hexagonal) crystal structure, verified in our study by XRD, can be considered. In the unit cell of La_2O_3 ($a = 3.147$, $c = 3.937$), each La ion is coordinated with seven oxygen ions: four with tetrahedral coordination, $O_{(t)}$, and three with octahedral coordination, $O_{(o)}$. By utilizing computer simulation, Islam *et al.* have calculated that the {001} and

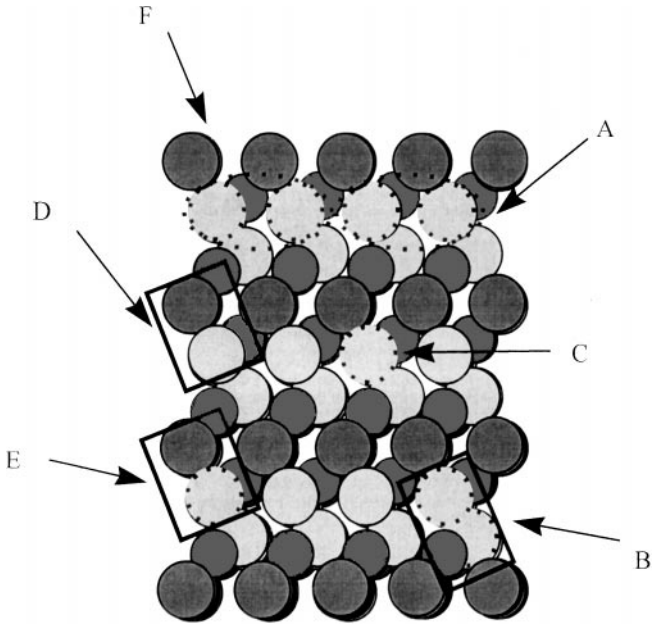

FIG. 22. La_2O_3 (011) surface: ○ oxygen at tetrahedral $O_{(t)}$ position; ●, oxygen anion at octahedral $O_{(o)}$ position; •, La cation. (A) Oxygen pair vacancy type I with an O–O distance of 397 Å; (B) oxygen pair vacancy type II with a shorter O–O distance of 2.88 Å; (C) single oxygen vacancy; (D) single vacancy plus adjacent surface lattice oxygen atom; (E) adjacent lattice oxygen atoms; and (F) coordinative unsaturated lattice oxygen atom at corner site.

{011} surfaces should dominate the equilibrium crystal morphology (39). The {001} surface is the most stable, with a slightly lower surface energy than the {011} surface. Furthermore, it has been predicted by Ilett and Islam that the formation of an $O_{(t)}$ vacancy is significantly more favorable than that of an $O_{(o)}$ vacancy (51). As shown elsewhere (11), both $O_{(t)}$ and $O_{(o)}$ atoms are exposed on the {011} surface, while only $O_{(o)}$ atoms exist on the {001} surface, with the exception of corner positions where $O_{(t)}$ atoms can be exposed; thus, oxygen vacancies should be more easily created on {011} surfaces. Figure 22 provides a model picturing the types of oxygen vacancy sites that can be created when La_2O_3 is conditioned at high temperature in He. The two types of oxygen pair vacancies can be recognized, one with an O–O distance of 3.94 Å (site A, type I) and the other with an O–O distance of 2.88 Å (site B, type II); however, the latter may only be generated at an edge position. The surface can also contain oxygen single vacancies, and it may be the different locations of the oxygen single vacancies that contribute to the different types of adsorbed NO species. The stable $(N_2O_2)^{2-}$ species are assumed to be formed only on type II oxygen pair vacancies with the shorter separation distance while N_2O at 300 K is produced at type I pair vacancies with the larger distance between the two oxygen atoms. The structure of *cis* hyponitrite ions, $(N_2O_2)^{2-}$, has been estimated to have an O–O separation of 2.4 Å, which is closest to the 2.88 Å distance in the type II sites. Both free NO_2^- and NO_3^- ions have O–O separation distances of approximately 2.1 Å; thus the chelated nitrites and bidentate nitrates may be more easily formed on the D and E sites, respectively, which have a shorter O–O separation distance of 3.1 Å compared to 3.97 Å in the type I sites.

Winter has proposed that NO decomposition on La_2O_3 occurs via the adsorption of two NO molecules on adjacent anion vacancies, each of which contains a trapped electron, followed by rupture of the N–O bonds to form N_2 and then desorption of O_2 (62). The proposal of the hyponitrite ion, $(N_2O_2)^{2-}$, as an active intermediate is supported by our IR studies in which NO^- and $(N_2O_2)^{2-}$ species are observed when NO is flowed over La_2O_3 at 800 K but are removed during a subsequent purge with Ar. This ion offers a better configuration to allow decomposition to N_2 and O_2 as it already has some N–N bond formation and the bond strength of N–O is weakened because the force constant is proportional to the square of ($\nu\nu_{NO}$) and the N–O stretching modes have been lowered to 1138 cm^{-1} ($\nu\nu_{a,N-O}$) and 820 cm^{-1} ($\nu\nu_{s,N-O}$) compared to values of 1876 cm^{-1} for neutral NO and 1195 cm^{-1} for NO^-.

Winter reported first-order dependencies for NO decomposition on La_2O_3 (62), whereas orders between 1 and 2 were reported by Vannice and co-workers (4). The mechanism proposed by Winter, which results in a first-order NO dependence in the derived rate expression, contains NO adsorption as the rate-determining step (RDS) and O_2 desorption as quasi-equilibrated. On the other hand, Vannice *et al.* have proposed a Langmuir–Hinshelwood sequence invoking a surface reaction between two adsorbed NO species as the RDS with NO adsorption and O_2 adsorption being quasi-equilibrated, and they derived a rate expression which allows the reaction order in NO to vary between 1 and 2 (4). The involvement of $(N_2O_2)^{2-}$ species is consistent with both models and, in particular, the La_2O_3 samples studied here were prepared exactly the same way as those examined by us previously (4). The $(N_2O_2)^{2-}$ species observed by DRIFTS at 800 K in the presence of NO, however, are more consistent with the latter model in which the NO adsorption step is very fast so that NO^- and $(N_2O_2)^{2-}$ species can accumulate on the surface. The rapid NO chemisorption at 300 K also indicates this is not a slow step; thus, our results do not support Winter's model. The breaking of N–O bonds can happen sequentially to form N_2O or it can happen to form N_2 directly since both sequences produce the same rate expression. Therefore, the mechanism for NO decomposition involving the sites proposed in our model of the surface can be represented as follows:

$$NO + (e^-|\square)(e^-|\square) \rightleftharpoons (NO^-_{ad}|\square)(e^-|\square) \quad [17]$$

$$NO + (NO^-_{ad}|\square)(e^-|\square) \rightleftharpoons (NO^-_{ad}|\square)(NO^-_{ad}|\square)\left(\text{or} \rightleftharpoons \square\left(N_2O_2\right)^{2-}\square\right) \quad [18]$$

$$(NO_{ad}^{-}|\square)(NO_{ad}^{-}|\square) \rightarrow (N_2O_{ad}^{-}\square)(O_{ad}^{-}|\square) \quad \text{(RDS)} \quad [19]$$

$$(N_2O_{ad}^{-}|\square)\left(O_{ad}^{-}|\square\right) \rightleftharpoons N_2 + (O_{ad}^{-}|\square)(O_{ad}^{-}|\square) \quad [20]$$

$$(O_{ad}^{-}|\square)\left(O_{ad}^{-}|\square\right) \rightleftharpoons O_2 + (e^{-}|\square)(e^{-}|\square). \quad [21]$$

If N_2 were to be formed without the involvement of an adsorbed N_2O species, steps [19] and [20] could then be combined into a single step. Regardless, $2NO \rightarrow N_2 + O_2$ is the overall reaction.

If the nitrate species were active intermediates, the presence of O_2 would be expected to enhance NO decomposition because it would facilitate nitrate; however, this supposition contradicts the result that O_2 retards NO decomposition (63). When NO was introduced at 700 K, not only was a larger amount of N_2O formed compared to that at 300 K, but also little N_2 was produced, and again this reaction ended quickly. Although oxygen can desorb from the surface at 700 K, gas-phase NO could rapidly interact with adsorbed O atoms left by the desorption of N_2 or N_2O and form stable nitrate species which would decompose only at 800 K or higher. This is consistent with the kinetics for NO decomposition over La_2O_3 which have shown that the reaction starts at about 800 K. Therefore, the catalytic route for NO decomposition appears to involve oxygen vacancies, particularly the pair sites on which two adjacent NO molecules can react to form N_2 or N_2O. The desorption of O_2 is required to regenerate the active centers and complete the catalytic cycle.

NO reacts rapidly with O_2 at 300 K to form NO_2 via Eq. [1]. From the TPD results, nitrate species are formed extensively since large amounts of NO and O_2 desorbed from 700 to 850 K. With the oxygen already activated in an NO_2 molecule, NO_2 is more easily adsorbed on the surface than NO. The amounts of NO and O_2 desorbed at high temperature were both about 10 μmol/m^2. If the morphology of La_2O_3 was assumed to consist mostly of {001} and {011} surfaces, as previously proposed, it can be estimated that on the {001} surface, which exposes only octahedral O atoms, $O_{(o)}$, the concentration of $O_{(o)}$ is 12.4 μmol/m^2, while the {011} surface contains 11.6 μmol/m^2 of tetrahedral $O_{(t)}$ and 5.8 μmol/m^2 of $O_{(o)}$. Thus, NO_2 adsorption may take place on any of the surface lattice oxygen atoms to form unidentate NO_3 species. This structure is similar to the unidentate carbonates formed after adsorption of CO_2 on La_2O_3 as proposed by Rosynek and Magnuson (12).

SUMMARY

Heating La_2O_3 at 973 K in He creates oxygen vacancies at the surface. Contacting this La_2O_3 surface with NO at 300 K produces N_2O and chemisorbed oxygen on the surface. Oxygen pair vacancies can be generated by desorption of molecular oxygen during a high-temperature pretreatment, and they can rearrange to form two single vacancies via migration of lattice oxygen at or near the surface. TPD of $^{18}O_2$ combined with the isotopic exchange reaction shows that oxygen adsorption is activated and dissociative and that the exchange reaction occurs on oxygen vacancies which can be occupied by adsorbed oxygen or NO. TPD of NO from a He-treated surface gives three distinct NO desorption peaks at 400, 700, and 800 K, with the latter peak always occurring concomitantly with O_2 desorption and giving an NO/O_2 ratio routinely near unity. Chemisorption of O_2 during cooling from 973 K prior to NO admission at 300 K inhibits the formation of N_2O and blocks sites for the NO desorption peak at 700 K, but enhances the 800 K peak. TPD of $^{15}N^{16}O$ adsorbed on a surface containing ^{18}O lattice ions, but no chemisorbed O atoms, showed that both $^{15}N^{16}O$ and $^{15}N^{18}O$ desorb at 400 K but only $^{15}N^{16}O$ is present in the 700 and 800 K desorption peaks, while TPD from a surface with both lattice and chemisorbed ^{18}O atoms showed that $^{15}N^{18}O$ desorbs at both 400 and 800 K. Consequently, the NO peak at 400 K involves exchange with surface lattice oxygen ions, while the 800 K peak involves exchange with chemisorbed oxygen atoms. DRIFT spectroscopy of NO adsorbed on La_2O_3 at 300 K showed that nitrosyl ions (NO^-), hyponitrite ions $(N_2O_2)^{2-}$, chelated nitrite (NO_2^-), nitrito (ONO^-), and bridging and monodentate nitrate species (NO_3^-) were present. The chelated nitrite, nitrito, and bridging nitrate species decomposed after heating of the sample to 473 K in Ar. Further heating to 673 K decreased the NO^- and $(N_2O_2)^{2-}$ species, and only monodentate nitrate species were seen after heating to 800 K. Consequently, the three NO TPD peaks are assigned as follows: 400 K, decomposition of nitrito, nitro, and bidentate nitrate species; 700 K, desorption of NO^- and $(N_2O_2)^{2-}$ species; and 800 K, decomposition of monodentate nitrate species into NO and O_2.

A model of the La_2O_3 surface based on the two lowest-energy crystal planes invokes six different sites: one oxygen pair vacancy which produces N_2O stoichiometrically 300 K; another oxygen pair vacancy on which hyponitrite $(N_2O_2)^{2-}$ species are formed; an oxygen single vacancy which forms anionic nitrosyl NO^- species; a single oxygen vacancy plus a lattice oxygen atom which forms a chelated nitrite species; two adjacent lattice oxygen atoms on which bridging nitrates are formed, and coordinatively unsaturated lattice oxygen atoms which allow nitrito species to form. The $(N_2O_2)^{2-}$ species are proposed to be an active intermediate in the NO decomposition mechanism, and they were detected under reaction conditions at 800 K by DRIFTS. Monodentate nitrates observed at 800 K appear to be too stable to be intermediates and therefore are spectator species.

ACKNOWLEDGMENTS

Support for this study was provided by the National Science Foundation under Grant CTS-9633752.

REFERENCES

1. Zhang, X., Walters, A. B., and Vannice, M. A., *Catal. Today* **27**, 41 (1996).
2. Zhang, X., Walters, A. B., and Vannice, M. A., *Appl. Catal. B* **4**, 237 (1994).
3. Huang, S.-J., Walters, A. B., and Vannice, M. A., *J. Catal.* **173**, 229 (1998).
4. Vannice, M. A., Walters, A. B., and Zhang, X., *J. Catal.* **159**, 119 (1996).
5. Klingenberg, B., and Vannice, M. A., *Appl. Catal. B* **21**, 19 (1999).
6. Cordatos, H., and Gorte, R. J., *Appl. Catal. B* **7**, 33 (1995).
7. Winter, E. R. S., *J. Catal.* **22**, 158 (1971).
8. Klingenberg, B., and Vannice, M. A., *Chem. Mater.* **8**, 2755 (1996).
9. Taylor, R. P., and Schrader, G. L., *Ind. Eng. Chem. Res.* **30**, 1016 (1991).
10. Lacombe, S., Geantet, C., and Mirodatos, C., *J. Catal.* **151**, 439 (1994).
11. Huang, S.-J., Ph.D. Thesis, The Pennsylvania State University, University Park, PA, 1999.
12. Rosynek, M. P., and Magnuson, D. T., *J. Catal.* **48**, 417 (1977).
13. Tsyganenko, A. A., Lamotte, J., Gallas, J. P., and Lavalley, J. C., *J. Phys. Chem.* **93**, 4179 (1989).
14. Bailes, M., Bordiga, S., Stone, F. S., and Zecchina, A., *J. Chem. Soc., Faraday Trans.* **92**, 4675 (1996).
15. Nakamoto, K., "Infrared and Raman Spectra of Inorganic and Coordination Compounds," Part B, 5th ed. Wiley, New York, 1997.
16. Davydov, A. A., and Rochester, C. H., "Infrared Spectroscopy on the Surface of Transition Metal Oxides." Wiley, Chinchester, 1994.
17. Busca, G., and Lorenzelli, V., *J. Catal.* **72**, 303 (1981).
18. Schraml-Marth, M., Wokaun, A., and Baiker, A., *J. Catal.* **138**, 306 (1992).
19. Ghiotti, G., and Chiorino, A., *Spectrochim. Acta. A* **49**, 1345 (1993).
20. Low, M. J. D., and Yang, R. T., *J. Catal.* **34**, 3479 (1974).
21. Nakamoto, K., "Infrared and Raman Spectra of Inorganic and Coordination Compounds." Part A, 5th ed. Wiley, New York, 1997.
22. Goubeau, J., and Laitenberger, K., *Z. Anorg. Chem.* **78**, 320 (1963).
23. Gee, N., Nicholls, D., and Vincent, V., *J. Chem. Soc.* 5897 (1964).
24. Cerruti, L., Modone, E., Guglielminotti, E., and Borello, E., *J. Chem. Soc., Faraday Trans. 1* **70**, 729 (1974).
25. Martinez-Arias, A., Soria, J., Conesa, J. C., Seoane, X. L., Arcoya, A., and Cataluna, R., *J. Chem. Soc., Faraday Trans.* **91**, 1679 (1995).
26. Shelef, M., and Kummer, J. T., *Chem. Eng. Prog. Symp. Ser.* **67**, 74 (1971).
27. Little, L. H., "Infrared Spectra of Adsorbed Species." Academic Press, London, 1966.
28. Snis, A., and Panas, I., *Surf. Sci.* **412/413**, 477 (1998).
29. Laane, J., and Ohlsen, J. R., *Prog. Inorg. Chem.* **27**, 465 (1980).
30. Davydov, A. A., Lokhov, Y. A., and Shakochikhin, Y. M., *Kinet. Katal.* **19**, 532 (1978).
31. Ekstrom, A., and Lapszewicz, J. A., *J. Am. Chem. Soc.* **110**, 5226 (1988).
32. Wang, J. X., and Lunsford, J. H., *J. Phys. Chem.* **90**, 3890 (1986).
33. Louis, C., Chang, T. L., Kermarec, M., Le Van, T., Tatibouet, J. M., and Che, M., *Colloids Surf. A* **72**, 217 (1993).
34. Yamashita, H., Machida, Y., and Tomita, A., *Appl. Catal. A* **79**, 203 (1991).
35. Dissanayake, D., Lunsford, J. H., and Rosynek, M. P., *J. Catal.* **143**, 286 (1993).
36. Sokolovskii, V. D., *Catal. Rev.-Sci. Eng.* **32**, 1 (1990).
37. Zhang, Z., Verykios, X. E., and Baerns, M., *Catal. Rev.-Sci. Eng.* **36**, 507 (1994).
38. Voskresenskaya, E. N., Roguleva, V. G., and Anshits, A. G., *Catal. Rev.-Sci. Eng.* **37**, 101 (1995).
39. Islam, M. S., Ilett, D. J., and Parker, S. C., *J. Phys. Chem.* **98**, 9637 (1994).
40. Winter, E. R. S., *J. Chem. Soc. (A)* 2889 (1968).
41. Winter, E. R. S., *J. Chem. Soc. (A)* 1882 (1969).
42. Hayes, W., and Stoneham, A. M., "Defect and Defect Processes in Nonmetallic Solids." Wiley, New York, 1985.
43. Lacombe, S., Zanthoff, H., and Mirodatos, C., *J. Catal.* **155**, 106 (1995).
44. Kalenik, Z., and Wolf, E. E., *Catal. Lett.* **11**, 309 (1991).
45. Kofstad, P., "Nonstoichiometry, Diffusion and Electrical Conductivity in Binary Metal Oxides." Wiley-Interscience, New York, 1972.
46. Etsell, T. H., and Flengas, S. N., *J. Electrochem. Soc.* **116**, 771 (1969).
47. Bogoroditskii, N. P., Pasynkov, V. V., Basili, R. R., and Volokobinskii, Y. M., *Sov. Phys.-Dokl.* **10**, 85 (1965).
48. Subba Rao, G. V., Ramdas, S., Mehrotra, P. N., and Rao, C. N. R., *J. Solid State Chem.* **2**, 377 (1970).
49. Borchert, H., and Baerns, M., *J. Catal.* **168**, 315 (1997).
50. Derbeneva, S. S., and Batsanov, S. S., *Dokl. Akad. Nauk. SSSR* **175**, 1062 (1967).
51. Ilett, D. J., and Islam, M. S., *J. Chem. Soc., Faraday Trans.* **89**, 3833 (1993).
52. Martinez-Arias, A., Soria, J., Conesa, J. C., Seoane, X. L., Arcoya, A., and Cataluna, R., *J. Chem. Soc., Faraday Trans.* **91**, 1679 (1995).
53. Yamashita, T., and Vannice, M. A., *Appl. Catal. B* **13**, 141 (1997).
54. Zecchina, A., Scarano, D., Bordiga, S., Ricchiardi, G., Spoto, G., and Geobaldo, F., *Catal. Today* **27**, 403 (1996).
55. Kung, M. C., and Kung, H. H., *Catal. Rev.-Sci. Eng.* **27**, 425 (1985).
56. Enemark, J. H., and Feltham, R. D., *Coord. Chem. Rev.* **138**, 339 (1959).
57. Indovina, V., Cordischi, D., Rossi, S. D., Ferraris, G., Chiotti, G., and Chiorino, A., *J. Mol. Catal.* **68**, 53 (1991).
58. Pozdnyakov, D. V., and Filimonov, V. N., *Kinet. Katal.* **14**, 760 (1973).
59. Yanagisawa, Y., *Appl. Surf. Sci.* **100/101**, 256 (1996).
60. Plater, E. E., Spoto, G., and Zecchina, A., *J. Chem. Soc., Faraday Trans. 1* **81**, 1283 (1985).
61. Driscoll, D. J., Martir, W., Wang, J.-X., and Lunsford, J. H., *J. Am. Chem. Soc.* **107**, 58 (1985).
62. Winter, E. R. S., *J. Catal.* **22**, 158 (1971).
63. Winter, E. R. S., *J. Catal.* **34**, 440 (1974).